UNIVERSITY OF SOUTHAMPTON
Faculty of Engineering and Physical Sciences
School of Electronics and Computer Science

A project report submitted for the award of
MEng Electronic and Electrical Engineering

Supervisor: Dr Ruomeng Huang
Examiner: Dr Abhinav Kumar Singh

Using Evolutionary Algorithm to optimise parameters of photonic radiator design

by Michael M. Southall

May 2, 2022

UNIVERSITY OF SOUTHAMPTON

ABSTRACT

FACULTY OF ENGINEERING AND PHYSICAL SCIENCES
SCHOOL OF ELECTRONICS AND COMPUTER SCIENCE

A project report submitted for the award of MEng Electronic and Electrical Engineering

by Michael M. Southall

Currently, there is insufficient research on materials and structures which utilises machine learning techniques for advancing the understanding of how to optimise parameters of photonic radiative coolers.

This project involves the use of an existing Python package called WPTherml, developed by researchers at William Paterson University. This programme is useful to the project, as it computes the thermal radiation spectra of planar multilayer structures via the Transfer Matrix Method (TMM).

After computing emissivity values via the TMM, this project's primary goal is to build a machine learning model with the goal of exploring the potential of using genetic algorithms to enhance understanding of how to optimise the thickness and materials used in radiative cooler design. The pool of materials that would be considered is largely dependent on what materials' optical properties data are readily available across the wavelength range of 200 nm to 20 μm. The implementation of genetic algorithms involves the use of a Python package called DEAP (Distributed Evolutionary Algorithms in Python) which is a computational framework for rapid prototyping of ideas that are based on evolutionary algorithms.

Statement of Originality

- I have read and understood the ECS Academic Integrity information and the University's Academic Integrity Guidance for Students.
- I am aware that failure to act in accordance with the Regulations Governing Academic Integrity may lead to the imposition of penalties which, for the most serious cases, may include termination of programme.
- I consent to the University copying and distributing any or all of my work in any form and using third parties (who may be based outside the EU/EEA) to verify whether my work contains plagiarised material, and for quality assurance purposes.

You must change the statements in the boxes if you do not agree with them.

We expect you to acknowledge all sources of information (e.g. ideas, algorithms, data) using citations. You must also put quotation marks around any sections of text that you have copied without paraphrasing. If any figures or tables have been taken or modified from another source, you must explain this in the caption and cite the original source.

I have acknowledged all sources, and identified any content taken from elsewhere.

If you have used any code (e.g. open-source code), reference designs, or similar resources that have been produced by anyone else, you must list them in the box below. In the report, you must explain what was used and how it relates to the work you have done.

I have not used any resources produced by anyone else.

You can consult with module teaching staff/demonstrators, but you should not show anyone else your work (this includes uploading your work to publicly-accessible repositories e.g. GitHub, unless expressly permitted by the module leader), or help them to do theirs. For individual assignments, we expect you to work on your own. For group assignments, we expect that you work only with your allocated group. You must get permission in writing from the module teaching staff before you seek outside assistance, e.g. a proofreading service, and declare it here.

I did all the work myself, or with my allocated group, and have not helped anyone else.

We expect that you have not fabricated, modified or distorted any data, evidence, references, experimental results, or other material used or presented in the report. You must clearly describe your experiments and how the results were obtained, and include all data, source code and/or designs (either in the report, or submitted as a separate file) so that your results could be reproduced.

The material in the report is genuine, and I have included all my data/code/designs.

We expect that you have not previously submitted any part of this work for another assessment. You must get permission in writing from the module teaching staff before re-using any of your previously submitted work for this assessment.

I have not submitted any part of this work for another assessment.

If your work involved research/studies (including surveys) on human participants, their cells or data, or on animals, you must have been granted ethical approval before the work was carried out, and any experiments must have followed these requirements. You must give details of this in the report, and list the ethical approval reference number(s) in the box below.

My work did not involve human participants, their cells or data, or animals.

Acknowledgements

I would like to thank my supervisor, Dr Ruomeng Huang who gave me great guidance to my first significant software project. In addition, I would like to thank my parents for their support.

Contents

List of Figures

List of Tables

List of Abbreviations

α	Absorptivity in the solar spectrum
COP26	2021 United Nations Climate Change Conference
DEAP	Distributed Evolutionary Algorithm in Python
ϵ	Emissivity in the atmospheric transparent window range
$GtCO_2$	Gigatonnes of carbon dioxide
GA	Genetic algorithm
HVAC	Heating, ventilation, and air conditioning
MIR	Mid-infrared range
ML	Machine Learning
n-k tables	Tables of refractive index (n) and extinction coefficient (k)
TMM	Transfer Matrix Method

Chapter 1

Introduction

Dealing with the consequences of the climate crisis is a pressing challenge that humanity faces. The report 'State of Climate 2021' by the World Meteorological Organisation was released during COP26. It stated that extreme heatwaves affected western North America during June and July, with many places breaking station records by 4 to 6 Celsius, causing hundreds of heat-related deaths [1]. The increase in frequency of heatwaves around the world causes the increased use of air-conditioning in order to mitigate the effects of extreme temperatures. Deschênes and Greenstone's study shows that the health of elderly and infants are most at risk in both extremes of hot and cold temperatures [2].

The increase in reliance of air conditioning systems causes an increase in electricity consumption. This leads to higher levels of greenhouse gases emitted into the atmosphere which, in turn, further exacerbates the problem of the increase in occurrence and intensity of extreme weather events. This vicious feedback loop highlights the importance of innovation in energy-saving technology, which improves on the efficiency of conventional Heating, ventilation, and air conditioning (HVAC) systems. Barreca et al., showed that the increased use in air-conditioning systems improves the households' probability in surviving hot days [3]. Thus, recent research interest in radiative cooling could have significant impacts on humanity's ability to cope with the immediate consequences of the climate crisis and the long-term sustainability of habitable conditions.

According to the International Energy Agency, energy-related CO_2 emissions from buildings have been flattening between 2013 and 2016. However, both direct and indirect emissions from electricity and commercial heat used in buildings rose to 10 $GtCO_2$ in 2019, the highest level ever recorded [4]. A large proportion of the

energy used is for indoor thermal management via conventional HVAC systems. Therefore, the energy-saving potential of traditional systems is huge.

A technology that could improve efficiency of existing systems is radiative cooling, which involves passively obtaining cooling energy by releasing heat of terrestrial-facing objects into the cold sink of outer space. By utilising the infrared atmospheric window ($8 - 13\ \mu m$) as the path of radiation heat transfer, a passive way of decreasing cooling energy requirements without additional power input could be realised. This specific wavelength range is important as it is where electromagnetic waves can travel though air without much absorption by atmospheric gases.

The development of photonic radiators and metamaterials has enabled significant technological advancements in innovative design and fabrication of radiators. The recent novel materials and structures of various radiators developed have created a new class of radiator – selective infrared radiators, which further highlights the advantages of diurnal radiative cooling. Despite these recent advancements, challenges remain which require further research. A challenge is to understand what materials and structures are best suited to incorporate into the multi-layered design of photonic radiators. Raman et al. demonstrated a planar photonic radiator which comprises of seven alternating layers of Hafnium dioxide and Silica with varying thickness on top of 200 nm thick Silver and 750 μm thick Silicon wafer substrate [5].

Currently, there is insufficient research on materials and structures which utilises machine learning for optimising parameters of photonic radiators. Hence, the primary goal is to explore the potential of using evolutionary algorithms to enhance understanding of optimising the thicknesses and materials used in radiator design. Specifically, under the umbrella of evolutionary algorithms, genetic algorithm is chosen for solving this optimisation problem.

Chapter 2

Background Research

2.1 Fundamentals of radiative cooling

A radiative cooler is subject to solar irradiance and atmospheric thermal radiation (corresponding to ambient air temperature, T_{amb}) [5]. Its cooling power is the difference between the power of the radiator and the power from the ambient atmospheric conditions, i.e. the sun, conduction and convection. A radiative cooler of area A, at temperature T, whose spectral and angular emissivity is $\epsilon(\lambda, \theta)$, the net cooling power is represented by:

$$P_{cool}(T) = P_{rad}(T) - P_{atm}(T_{amb}) - P_{sun} - P_{cond+conv} \tag{2.1}$$

where the power radiated out by the structure is:

$$P_{rad}(T) = A \int d\Omega cos\theta \int_0^\infty d\lambda I_{BB}(T, \lambda)\epsilon(\lambda, \theta) \tag{2.2}$$

$$\int d\Omega = 2\pi \int_0^{\frac{\pi}{2}} d\theta sin\theta \tag{2.3}$$

where (2.3) is the angular integral over a hemisphere.

$$I_{BB}(T, \lambda) = \frac{2hc^2}{\lambda^5} \frac{1}{e^{\frac{hc}{\lambda k_B T}} - 1} \tag{2.4}$$

where (2.4) is the radiance of a blackbody, where h is Planck's constant, k_B the Boltzmann constant, c is the speed of light and λ is the wavelength.

$$P_{atm}(T_{amb}) = A \int d\Omega cos\theta \int_0^\infty d\lambda I_{BB}(T_{amb}, \lambda)\epsilon(\lambda, \theta) \tag{2.5}$$

Equation (2.5) is the absorbed power due to incident atmospheric thermal radiation, while equation (2.6) is the incident solar power absorbed by the structure:

$$P_{sun} = A \int_0^\infty d\lambda \epsilon(\lambda, \theta_{sun} I_{AM1.5}(\lambda)) \tag{2.6}$$

In equation (2.6), the solar illumination is represented by $I_{AM1.5}(\lambda)$, the $AM1.5$ spectrum. An assumption is made that the structure is facing the Sun at a fixed angle θ_{sun}. Therefore, the term, P_{sun}, does not have an angular integral, and the structure's emissivity is represented by its value at θ_{sun}.

$$P_{cond+conv}(T, T_{amb}) = Ah_c(T_{amb} - T) \tag{2.7}$$

where $h_c = h_{cond} + h_{conv}$.

Equation (2.7) represents the power lost due to convection and conduction, where h_c represents a combined non-radiative heat coefficient that captures the effect of conductive and convective heating [5].

2.2 Challenges of radiative cooling design

An important concept is the intrinsic cooling loss of the radiator. This concept takes into account the effect of radiation, conduction and convection. In particular, conduction and convection heat transfer are the main mechanisms of the process of cooling loss. Therefore, it is a crucial factor that affects the performance of a radiator.

For instance, when the ambient temperature is lower than the temperature of the radiator, the radiator has a negative cooling loss power. This leads to an increase in the overall cooling power. Conversely, the cooling loss process has a detrimental effect on the minimum temperature the radiator can reach in a sub-ambient radiative cooling setting.

Radiative coolers radiate heat to outer space while reflecting solar irradiation as shown in the basic energy flow of a radiative cooler in Figure 2.1(a) [6]. Therefore, optimising the radiator's spectrum in both solar (shown by Figure 2.1(b)) and thermal wavelength range is crucial to achieve high cooling power. Figure

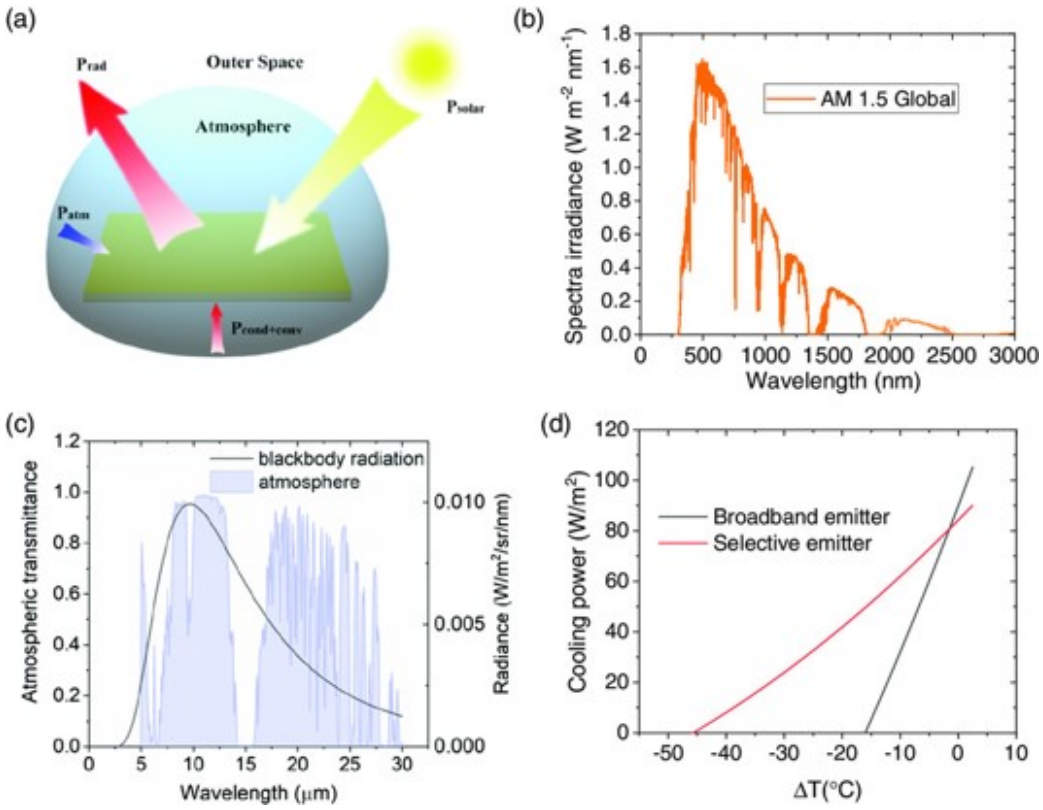

FIGURE 2.1: a) Schematic diagram of the energy flow of a radiative cooler; b) Spectral distribution of the AM 1.5 Global solar irradiation; c) Atmosphere transmittance and the blackbody radiation spectra under the temperature of 300 K; d) Cooling power of the two typical emitters: broadband emitters and selective emitters [6].

2.1(c) shows the radiation of a blackbody which serves as a good reference point when designing structures of radiators. Lastly, Figure 2.1(d) shows a comparison of cooling power achieved between a selective emitter and a broadband emitter. Importantly, material dispersion is a challenging problem to consider when optimising for broadband emitters.

Some previous studies apply an assumption that materials have a non-dispersive characteristic when optimising photonic structures. This assumption holds for narrowband emitters but it may not hold when designing broadband emitters as refractive indices of materials can differ markedly in the consideration of a wider wavelength range. As a result, the complexity of optimising the target spectrum for broadband emitters increases. This is where integrating a Genetic Algorithm (GA) into the optimisation process is beneficial.

A comparison between target spectral emissivity of a selective emitter (i.e. emitter A), and a broadband emitter (i.e. emitter B) is shown in Figure 2.2 [7]. The green line represents the ideal spectrum of a selective radiator with high emissivity only

within the infrared atmospheric window. Conversely, the orange line represents the ideal spectrum of a broadband with high emissivity in the entire mid-infrared range (MIR) (i.e., over 4 μm). Having high emissivity in the MIR is vital for

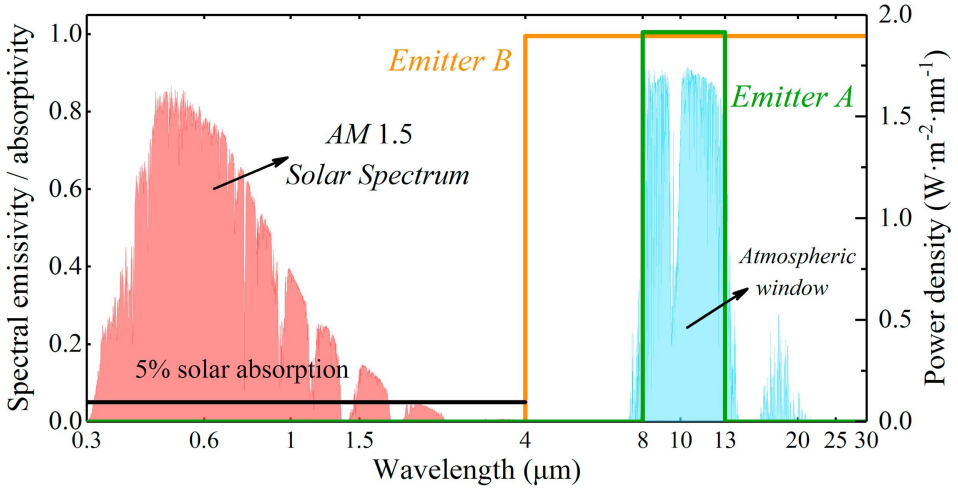

FIGURE 2.2: Radiative properties of different radiators, with AM 1.5 solar spectrum and a typical atmospheric window plotted as reference [7].

maximising the efficiency of the radiative cooler. If achieving day-time radiative cooling under solar irradiation is the objective, having low absorption in the solar spectrum is key. A range of possible solutions have been extensively studied, including the use of photonic crystals, multilayer film, optical metamaterials and polymeric materials [8]. Although certain polymers have excellent potential due to their infrared emissivity and transparent characteristic in the visible spectrum, they are prone to degradation in outdoor scenarios [9]. The use of metamaterials with subwavelength structures to obtain an ideal emissivity spectrum is achievable. However, this class of material requires complex fabrication processes which make utilising metamaterials unfeasible in practice [10]. The increase in complexity causes scalability issues in fabrication techniques which drive up the cost of manufacturing. Hence, this project omits analyses that rely on the use of polymers and metamaterials in multilayer photonic structures.

M. Kim et al., recently published an optimisation of a multiplayer structure study which involved selecting ten candidate materials - Al_2O_3, $BaTiO_3$, Cu_2O, hBN, Si_3N_4, SiC, SiO,SiO_2, $SrTiO_3$, and TiO_2 [8]. This consideration depended on three main factors. Firstly, the chosen materials should have significant differences in their refractive index values across the solar spectrum. This factor is important as inducing a mismatch of impedance in order to increase solar reflectivity is vital to achieve day-time radiative cooling. Secondly, the selected materials should have a high value of extinction coefficient in the wavelength range of the infrared

atmospheric window. Refractive index data is displayed n-k tables. It derives from the velocity of propagation of an electromagnetic wave through a solid, where the frequency-dependent complex refractive index N, is shown by the equation $N = n - ik$. The real part of this equation relates to the velocity while the imaginary part, called the extinction coefficient, relates to the damping of the oscillation amplitude of the incident electric field. The final factor was feasibility of fabrication so metamaterials and other types of material that require complex fabrication techniques were omitted from the study.

2.3 Fundamentals of Genetic Algorithm

Optimisation of multilayer photonic structure is difficult due to the high computational cost of evaluating the performance for all possible combination of materials and thicknesses. In addition, the parameter space generally includes many local minima, which makes deterministic optimisation schemes that search for the global minima unfeasible. To overcome these difficulties, a range of different algorithms have been explored by researchers when optimising design features of optical thin-film structures, such as Genetic algorithm (GA), Memetic algorithm, Differential Evolution and Particle Swarm Optimisation [11].

This project explores the potential of using GAs to optimise a range of different multilayer structures with different thicknesses. GAs could be useful for this optimisation problem as it is typically feasible for problems that contain multiple input parameters.

The concept of GA falls under the branch of algorithms called Evolutionary Algorithms. This specific type of Evolutionary Algorithm mimics the real-life process of biological evolution based on natural selection. In the natural world, the evolutionary process typically starts with a species producing more individuals than needed to ensure the survival of its species. This leads to a population of individuals that has a range of different characteristics. Some environmental factors cause certain individuals to survive longer, and thus can reproduce more than others. The consequence is that the characteristics of those individuals who are more adept at surviving become more common in the population over time. To translate this scenario to a computational model, several variables are needed – a fitness function of a population, selection, crossover and mutation mechanisms.

There is a wide range of options that could be considered when experimenting with the mentioned mechanisms. For instance, any fitness function can be experimented as long as it includes a quantitative measure that can represent how fit an individual is. As a specific example, a fitness function could be the maximisation of the cooling power of the radiative cooler when the goal is to find the ideal multilayer structure.

Moreover, a common selection process is the Tournament Selection. This method starts with a random selection of individuals which leads to a competition between the selected individuals. Crucially, every individual has the same probability of being selected, which ensures that there is diversity in the resultant population. The number of individuals selected for each tournament is referred as the tournament size. Typically, the tournament size is set as two due to its efficiency, but this parameter could be set as any positive integer.

A prevalent crossover mechanism is the one-point crossover method. This involves selecting a point along the chromosomes of both parents and swapping the split portions of the genes to form two children that contain a mix of both parents' chromosomes. This designated point where the gene is split is referred to as the crossover point. Researchers may experiment with having more than a single crossover point in which the method is logically named as the k-point crossover technique, where k could be any positive integer.

The mutation mechanism typically begins after the crossover process. A common method used is the Bit-flip mutation technique. This technique involves selecting one or more random bits and subsequently flipping them. Including a mutation mechanism in the design of GA is vital as this inclusion could prevent the model getting stuck at a local optimum, as it increases the diversity of the pool of individuals.

In this project, the goal is to utilise the combination of the TMM and GAs to define the materials used, the order and the thicknesses of layers, with the use of different fitness functions so that the validity of fitness functions can be compared.

A similar approach using TMM with GA has been explored by P. You, X. Li, et al. recently [10]. This 2020 study designed an optimised coating with 1.5-μm-overlapping MgF_2 and Si_3N_4 layers on top of a Silver film. The design achieved a net cooling power of $62W/m^2$ under ambient air temperature and a temperature reduction of 6.8 Celsius below ambient, when the ambient temperature is 300 K. Compared to previous studies, the total thickness of the designed coating of 1.5

μm is thinner. This design achieves 130 % radiative cooling power with only 75% thickness compared to Raman et al.'s multilayer film design in 2014.

However, there are several factors in which this project differs from the study mentioned above. Firstly, P. You et al.'s study implemented a fitness function of radiative cooling power density, while this project consists of exploring different fitness functions and evaluating the strengths and limitations of them. Moreover, the most important difference is that P. You et al.'s study selected Magnesium fluoride (MgF_2) and Silicon nitride (Si_3N_4) as dielectric materials in the optimisation strategy before the optimisation of the structural parameters due to their spectral properties [10]. The author's methodology on the other hand, consists of selecting a larger pool of candidate materials, but will include MgF_2 and Si_3N_4 in this pool due to their suitable spectral properties as mentioned.

Chapter 3

Design and Implementation

3.1 Verification of WPTherml

Although the three factors under the material selection consideration mentioned in the study conducted by M. Kim et al. in Section 2.2 were valid, there are further constraints to this project. A significant challenge initially was to find sufficient refractive index data for the wavelength range of 200 nm to 20 μm. Therefore, the pool of materials that this study could include is heavily dependent on retrieving sufficient, good quality n-k data. To attain data, the website - 'refractiveindex.info' was used due to its clear citations of the academic sources of n-k tables [12].

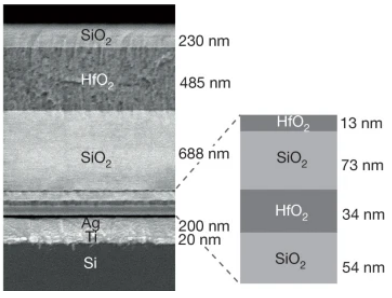

FIGURE 3.1: Planar photonic radiator which comprises of seven alternating layers of Hafnium dioxide and Silica with varying thickness on top of 200 nm thick silver and 750 μm thick Silicon wafer substrate [5].

Despite having optical data for a wide range of materials, a process of combining n-k data from numerous academic papers was needed to satisfy the goal of covering the 200 nm to 20 μm wavelength range. This combination of data was done via '.txt' files which were integrated into an existing Python package called

WPTherml. This package is a computational engine for simulating optical properties of nanostructures made from layered isotropic media and was released in 2019 by J. Varner et al. [13]. It is an ideal tool as the programme computes the thermal radiation spectra of planar multilayer structures via the Transfer Matrix Method (TMM).

After adding '.txt' files of the n-k data of Silicon carbide and Calcium fluoride, additional functions were added to the existing 'datalib.py' file so that the programme could recognise the new materials when running simulations. Although there is n-k data that covers the initial target wavelength range of 200 nm to 20 μm for the mentioned materials, the n-k data for several materials did not cover the entire range. Fortunately, after taking the fitness functions that the author plans to investigate into consideration, the upper limit of n-k data of 20 μm is reduced to 13 μm. Thus, more materials could be added to the pool of candidate materials. The explanation of what fitness functions are used will be in later sections.

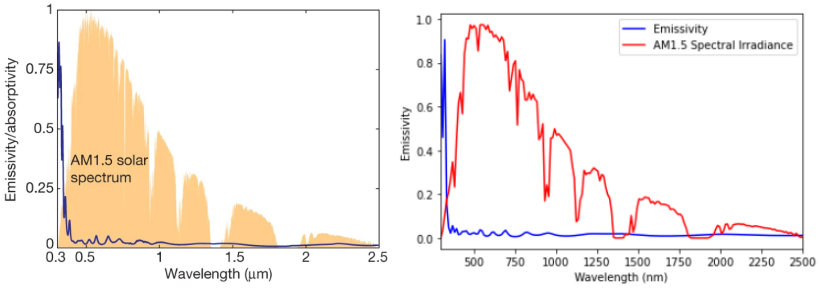

FIGURE 3.2: Side by side comparison of emissivity versus wavelength plots $(0 - 2.5\mu m)$ from Raman et al.[5] paper (left), and the same plot reproduced with the use of WPTherml package (right).

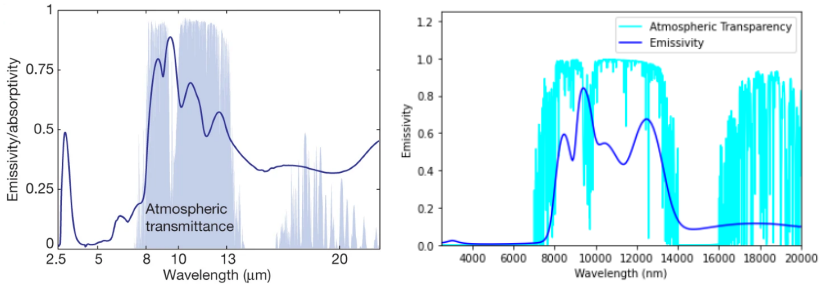

FIGURE 3.3: Side by side comparison of emissivity versus wavelength plots $(2.5\mu m - 20\mu m$) from Raman et al.[5] paper (left), and the same plot reproduced with the use of WPTherml package (right).

To familiarise with WPTherml and verify that the calculations based on the TMM matches with photonic designs from previous research, a reproduction is done on emissivity versus wavelength plots based on the planar photonic structure in Figure

3.1 Raman et al. developed [5]. In addition, Figure 3.2 and 3.3 shows side by side comparisons of emissivity versus wavelength plots from Raman et al. paper [5], and the same plots reproduced with the use of WPTherml package. Figure 3.2 consists of graphs that have a wavelength range of 0 to 2.5 μm and shows the AM1.5 solar spectrum. While Figure 3.3 consists of graphs that have a wavelength range of 2.5 nm to 20 μm and shows the infrared atmospheric window which sits between the wavelength range of 8 μm and 13 μm.

3.2 Design and implementation of ML model

Materials selected in the pool of candidate materials and their corresponding thicknesses are parameters to be optimised by the GA. These parameters are represented by chromosomes which are strings of binary numbers that are divided into portions. Each portion represents a gene (i.e. a set of chromosomes) which points to a parameter. For example, when dealing with the gene that represents the thickness parameter, an arbitrary range of thickness between $100nm$ to $1000nm$ with a $20nm$ step could be set. In this case, this range would mean there are 50 steps which could be represented as '110010' in binary numbers. As $2^6 = 64$, this confirms that strings of six binary numbers are sufficient in this example.

The process of the ML model and how it links with WPTherml's TMM computation tool is shown in Figure 3.4.

Firstly, a population which is defined as a group of individuals is initialised. Each individual is represented in a string of binary numbers which are generated randomly at the initialisation process. A conversion mechanism needs to be developed to convert the strings of binary numbers into material names and numerical thicknesses so that WPTherml can read the input parameters.

After the initial population is evaluated by a fitness function, a selection, crossover, and mutation mechanisms start. As the strings of binary numbers alter, the materials and thicknesses are updated and consequently re-evaluated by the fitness function. Then, the process reaches to the termination condition of the generation stage where the process loops back to the 'selection, crossover and mutation' stage if the condition is not satisfied. If the termination condition is satisfied, the best multilayer structure in the generation is stored in an array and reaches the iteration termination condition stage. If the termination condition is not fulfilled,

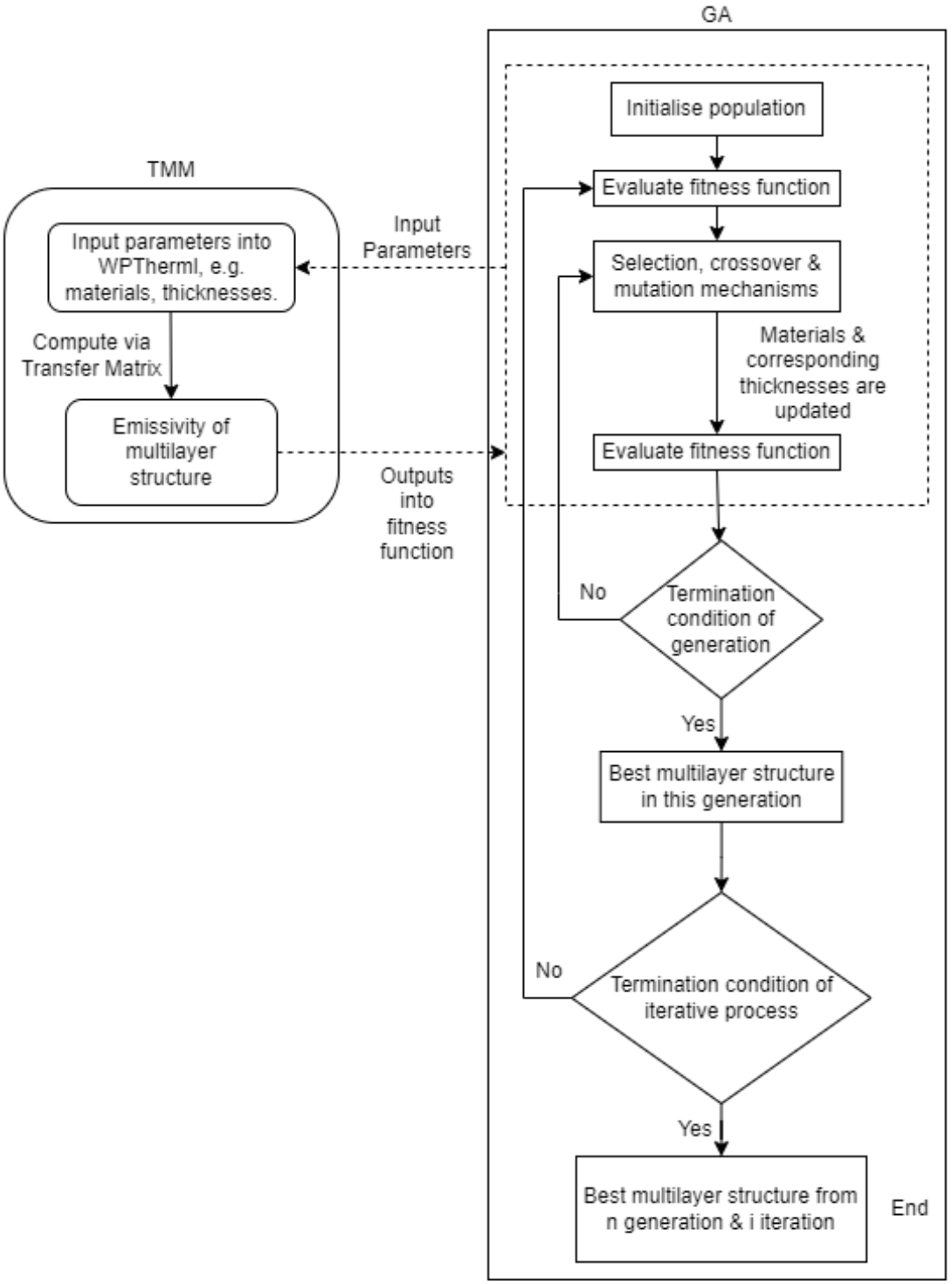

FIGURE 3.4: Flow chart of proposed machine learning model which combines TMM and GA.

the process is looped back to the evaluation of fitness function stage. Lastly, if the condition is reached, the model ends as the optimal multilayer structure is found.

A termination condition could be set as anything but a common example would be based on the limitation of processing time of the computer.

Before implementing a GA which takes in multiple parameters with a large pool of candidate materials, a logical approach consisted of implementing a simpler version which takes in only one parameter. In this case, a simplified model involving four materials with fixed thicknesses was developed before adding layers of complexities on this foundational work. This simplified model was completed in Semester 1 but it can not be used for any testing due to its simplicity. Therefore, the majority of Semester 2 was spent building a model that supports four candidate materials and a range of thicknesses.

Taking into account computational time and the ability for the model to generate representative results, the range of thicknesses that each layer of material could have was elected to be 100 nm to 2 μm, with a resolution of 10 nm. The upper limit of 2 μm for each layer is to ensure that the final multilayer structure would not be too thick. Each thickness is generated by a random number generator. Once the model of four candidate materials is proven to be able to generate valid results, a scale up of the model which supports a larger number of materials will be tested.

Although the initial plan involved chromosomes that are encoded in binary numbers, a revised method with decimal numbers was implemented in the first simplified model. This is because a Python package called Distributed Evolutionary Algorithms in Python (DEAP) supports decimal representation [14]. This additional support feature makes binary representation less effective as this system would require additional processes for encoding and decoding chromosomes.

A simplified example with three candidate materials is as follows. As the base layer of the multilayer structure should be a reflector, the position of a Silver layer is fixed , while the three remaining candidate materials could be rotated in any layer above the Silver base. In this example, the three materials investigated are Calcium fluoride, Hafnium oxide and Silicon carbide, which are represented by ‘0’, ‘1’, and ‘2’ respectively. For instance, a structure with Hafnium oxide sandwiched between Silicon carbide (top layer) and Calcium fluoride, with Silver at the bottom was stored in a list - [2, 1, 0]. A random number generator is used to ensure that the material layers are ordered randomly. As mentioned, the model used to generate representative results involves more candidate materials, but this simple example explains how the model is implemented.

3.2.1 Fitness function consideration

A good radiative cooler has a strong thermal emission in the atmospheric transparent window range (8 μm to 13 μm) while having minimal absorption in the solar spectrum range (0 to 2.5 μm)[8]. The emissivity in the atmospheric transparent window range is denoted by ϵ and the absorptivity in the solar spectrum range is represented by α. Therefore, this project consists of investigating the suitability and performances of the fitness functions $\epsilon \div \alpha$ and $\epsilon - \alpha$. Note that the theoretical maximum fitness value from $\epsilon - \alpha$ is 1 as the perfect radiative cooler would achieve an ϵ value of 1 (i.e. maximum thermal emission) and an α value of 0 (i.e. no solar absorption). There is no theoretical upper limit for fitness values from $\epsilon \div \alpha$ as it consists of a division.

3.2.2 Materials in candidate pools

The inclusion of MgF_2 and Si_3N_4 in the candidate material pool is primarily justified by P.You et al.'s study as mentioned at the end of Section 2.3 [10]. While the inclusion of HfO_2 and SiO_2 and the decision to use Silver as the base reflective layer are justified by the well-known Raman et al. study [5]. Furthermore, the inclusion of Al_2O_3, SiC and TiO_2 is justified by M.Kim et al's recent GA optimisation study [8]. Finally, the inclusion of CaF_2 is justified by Y. Huang et al. GA study [15].

Importantly, the justifications mentioned are simply the primary justification, all materials investigated are commonly used in recent literature. The first model's candidate pool of four materials consist of CaF_2, Al_2O_3, Si_3N_4 and SiO_2. The selection of including specific materials first, and only including others in larger candidate pools is arbitrary. This is because the objective is to investigate the parameters of GA, not identifying what materials are more likely to create the best multilayer radiative cooler.

Chapter 4

Testing methodology and Results

4.1 Introduction of methodology

In G. Ochoa et al., researchers stated that a GA's performance depends heavily on the choice of its main parameters: mutation rate, crossover rate, and population size [16]. Crucially, the relationships between these parameters are nonlinear. Thus, it is not possible for them to be independently optimised. This is the fundamental reason for this project.

Optimal GA parameter settings have been studied by many researchers, but there is no consensus on what is best [16]. Most studies in the 1990s focused on finding optimal mutation probabilities, while neglecting the variable of crossover probability in order to simplify the analysis. Before the 1990s, they involved using a rigid set of test problems to search for optimal parameters. The limitation of these studies is the inability of these findings to form general guides that could be applied universally with high accuracy.

The first parameter to investigate when collecting data from the simulation is population size. Theoretically, the larger the population size, the more likely the GA could arrive at a higher fitness value. This is intuitive as the probability of an individual having a high fitness value increases when there are more individuals to choose from. Despite this obvious relationship between these two factors, it is good practice to verify it in the particular use case of optimising multilayer structures as the optimal population size could vary between different use cases. Also, identifying the optimal population size is a key first step due to the significant trade-off between population size and computational time of the GA.

E. Williams et al. aimed to produce guidelines for empirically deriving optimal population size and mutation rate [17]. This paper presented the challenge of finding an optimal population size for any given problem. It stated that large population size provides good coverage of the design space but risks being excessively diverse that it is statistically difficult to combine two individuals with high fitness values to generate near-optimal offsprings. Conversely, a small population size may not provide enough diversity for the GA to discover designs close to the global optimum and will prematurely converge.

It is important to note that while some projects would have a fixed methodology prior to the start of the experimentation process and therefore having separate sections for methodology and testing would be reasonable, this is not the case for this project. As GA has many parameters, and the optimal settings for these parameters are not known at the beginning of testing, the logical approach would involve forming assumptions for parameters at the initial phase and test each parameter by varying one parameter at a time while having all other parameters fixed. Due to the nature of manually tuning parameters, the testing methodology is adjusted while running simulations. As both the results of simulations and past academic papers will be used to justify the continuous evolution of the testing methodology, Chapter 4 consists of the combination of methodology and results of simulations.

Initially, all simulations focus on finding optimal parameters for the GA that is based on the $\epsilon - \alpha$ fitness function. Subsequently, comparisons on GA performances will be made between the $\epsilon - \alpha$ and $\epsilon \div \alpha$ fitness functions.

4.2 Justification of population size parameter

Figure 4.1 shows a comparison of the average fitness values based on the $\epsilon - \alpha$ fitness function over fifty generations between five different population sizes. All five curves follow the typical GA shape where the average fitness values increase significantly initially from around the 3^{rd} to the 10^{th} generation. Each curve then reaches a plateau and fluctuates within a narrow range of average fitness values. Although population sizes of 20 and 50 would rarely be considered to use in any GA, these small sizes are included to highlight the significant increase in average fitness value as the population size is increased to 80 and above. The three plateaus of population size 80, 100 and 200 being significantly higher than the lower two population sizes is clear in Figure 4.1.

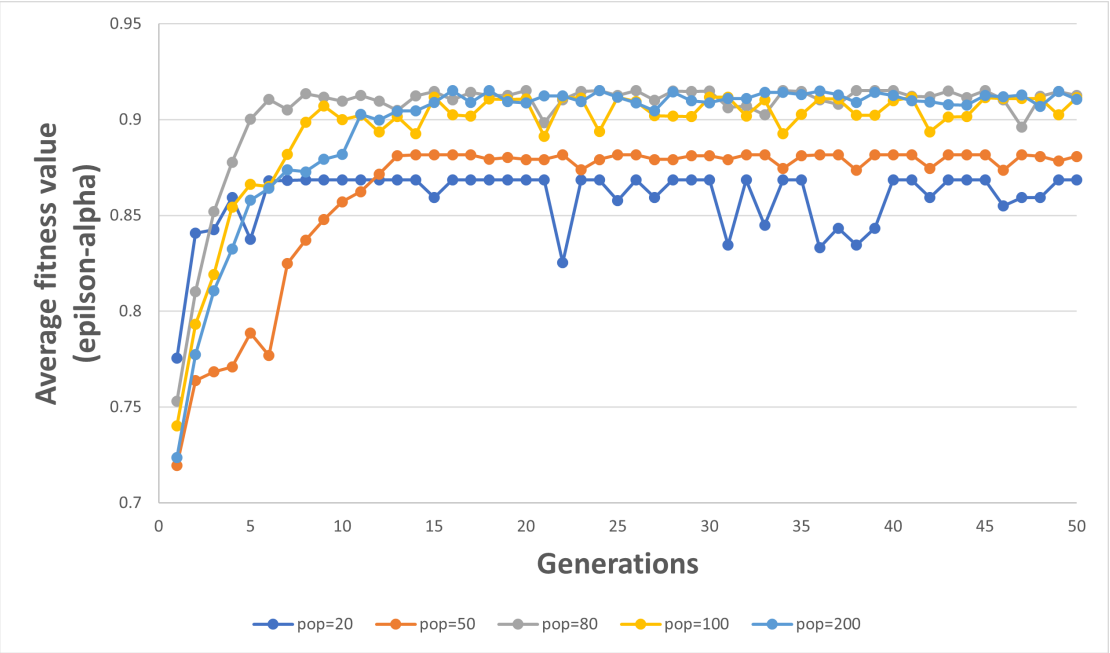

FIGURE 4.1: Justification of population size: A comparison of the average fitness values based on the $\epsilon-\alpha$ fitness function over fifty generations between five different population sizes. Population sizes of 80 and above perform significantly better than sizes of 20 and 50.

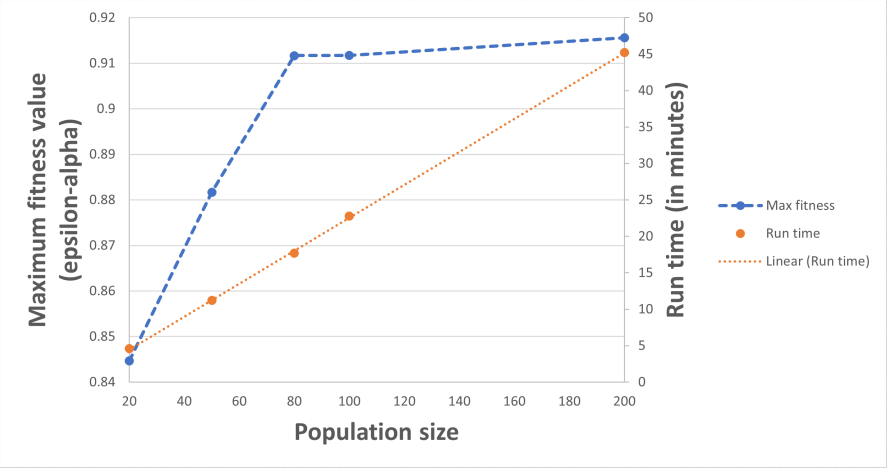

FIGURE 4.2: Justification of population size: Maximum fitness values (left y-axis) and simulation run time (right y-axis) against population sizes plot. Population size of 80 is identified as the optimal size and will be used in all following simulations.

The blue curve representing maximum fitness values in Figure 4.2 shows that they increase dramatically after fifty generations as the population size increases from 20 to 80. While the increase of population size from 80 to 200 has negligible change in maximum fitness values. Therefore, all following GA simulations use the population size of 80. The orange curve shows that the increase in computational time is directly proportional to the increase in population size. Thus, by choosing the

population size of 80 instead of a larger size would significantly reduce computation time while producing similarly representative results. Reducing run time for each simulation is important due to the need to run a large number of simulations when investigating multiple GA parameters.

4.3 Optimisation of crossover & mutation rates

4.3.1 Introduction

A.J. Umbarkar et al.'s stated that many researchers have a rule of thumb that the value of crossover probability is usually between 0.6 and 1 [18]. However, there are several dependencies. Firstly, it depends on the type of crossover used for which there is a huge amount to choose from. A.J. Umbarkar et al.'s review paper alone covered twenty different types of crossover operators. Secondly, although increasing crossover probability leads to an increase in the opportunity for recombination by definition, this increase could disrupt the occurrence of good combinations. Lastly, standard crossover can have high chance to produce illegal offspring, depending on the chosen encoding method.

Crucially, all points mentioned above depends on the specific application. This is the fundamental reason why GA optimisation is difficult. There is general rule of thumb as mentioned, but the effects of all parameters vary by application. As a result, this study consists of manually tuning GA parameters to analyse what parameters are likely to perform better for the specific use-case of designing multilayer radiative coolers. As mentioned in previous sections, due to the user-friendliness of the DEAP python package, it supports any encoding method. Therefore, to avoid introducing complexities unnecessarily, the author chose not to convert decimal representation of different materials and thicknesses to other encoding methods such as binary encoding.

Reviewing several papers on crossover and mutation probabilities for common computer science problems such as the Travelling Salesman Problem, is useful to give the author a general direction of how to manually tune GA parameters. However, there are a few recent studies where researchers applied GA to the specific use-case of optimising multilayer photonic structures. Therefore, these papers will be focused more heavily due to the application-specific nature of GA. They will form the bulk of the supporting material that justifies the author's methodology of analysing GA parameters and forming conclusions of what parameters are optimal.

4.3.2 Simulation results of crossover rate parameter

The methodology for searching for the optimal crossover probability consist of running tests that cover a wide range of crossover rates while keeping all other parameters fixed. As mentioned in the introduction section, A.J. Umbarkar et al. summed up that researchers usually select a crossover rate of between 0.6 to 1 [18]. Although the author could make this assumption and run tests that solely cover this range of crossover rates, it is decided that the tests would cover the crossover probability range of 0.2 to 0.8. Firstly, this is because the more important factor to take into account is the application dependence of GA parameters. This means that following a rule of thumb and immediately discarding the potential that lower crossover rates might produce better fitness values is a poor choice.

Furthermore, even if the crossover analysis ends up fitting the rule of thumb, it is useful for the author to understand to what extent the lower crossovers rates lead to inferior fitness values. The difference in performance is likely to be significant based on previous studies but there remains the possibility that the lower crossover rates could lead to inferior fitness values but in a negligible magnitude. This comparison of the wider range of crossover rates also enables the author to verify that the higher crossover rates do indeed lead to higher GA performance and to understand the magnitude of the difference in performance.

Figure 4.3 shows the comparison of crossover probabilities by plotting average fitness values based on the $\epsilon - \alpha$ fitness function against the number of generations. All four curves are based on the average of five test cycles. This repetition of tests ensure that the random nature of GA is taken into account. The four curves all fit the typical GA performance shape of a rotated letter L, where there are significant increases of average fitness values from the first generation to around the 6^{th} to 8^{th} generation. At approximately the 10^{th} generation, the curves hit a plateau and the average fitness values then oscillate within a narrow range. Moreover, it is clear that the crossover rate of 0.2 (blue curve) performs significantly poorer compared to higher rates. Although the curve of crossover rate 0.4 clearly oscillates at a lower level compared to the rates of 0.6 and 0.8, the difference in performance is not clear, especially for 0.6 and 0.8 crossover rates.

This lack of clarity leads to the need for Figure 4.4. Instead of comparing the average fitness values over 50 generations, Figure 4.4 compares the maximum fitness value after 50 generations. The methodology of repeating the tests for five cycles remains the same. Useful conclusions could be made by analysing

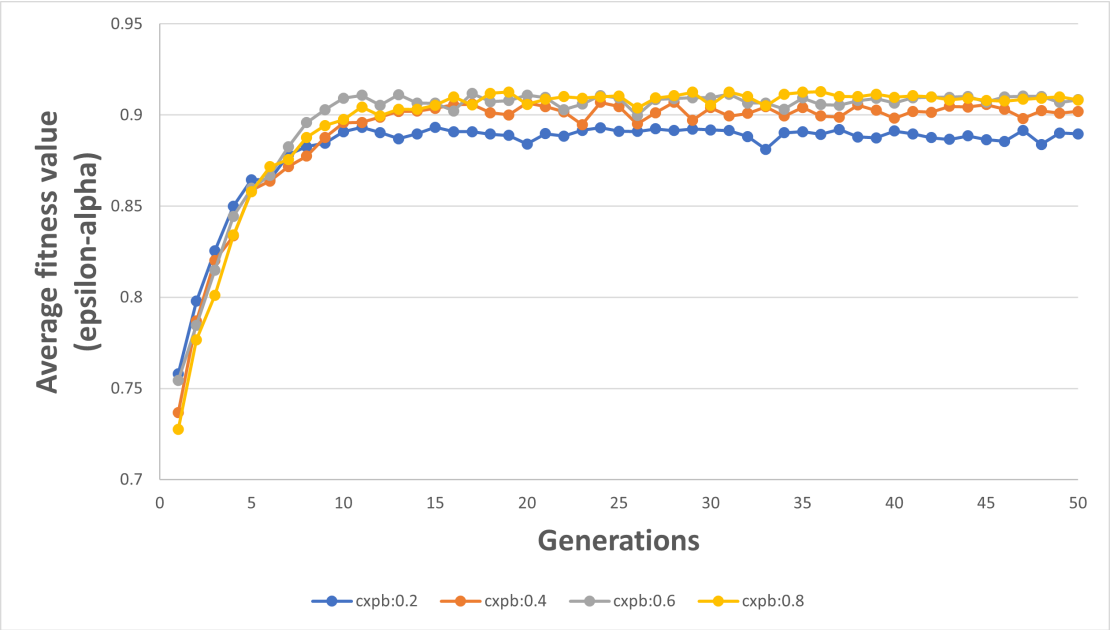

FIGURE 4.3: Comparison of different crossover probabilities (cxpb): Average fitness values base on the $\epsilon - \alpha$ fitness function against the number of generations. All four curves are based on the average of five test cycles. Crossover rates of 0.2 and 0.4 perform significantly worse than higher rates but more evidence is needed to distinguish performance differences in 0.6 and 0.8 crossover rates.

Figure 4.3 in conjunction with Figure 4.4. Firstly, the significantly lower average maximum fitness value when using the crossover probability of 0.2 matches with the significantly lower plateau level of the blue curve in Figure 4.3. Moreover, the closeness in performance shown by the proximity of the curves of crossover rates 0.4, 0.6 and 0.8 in Figure 4.3, matches the relatively close average maximum fitness values of the same crossover rates in Figure 4.4.

The performance between crossover rates of 0.6 and 0.8 is even closer. This is shown in Figure 4.3 where the grey curve (crossover probability of 0.6) and the yellow curve (crossover probability of 0.8) oscillates at an extremely similar plateau level and the curves often overlap each other over 50 generations. This similarity in performance is confirmed by Figure 4.4 where both average maximum fitness values for crossover probabilities of 0.6 and 0.8 lie within the range of 0.91 and 0.915.

To conclude, as the average maximum fitness value for crossover probability 0.8 over five test cycles is the highest, the optimal crossover probability is concluded to be 0.8. This crossover rate will be used in all following tests.

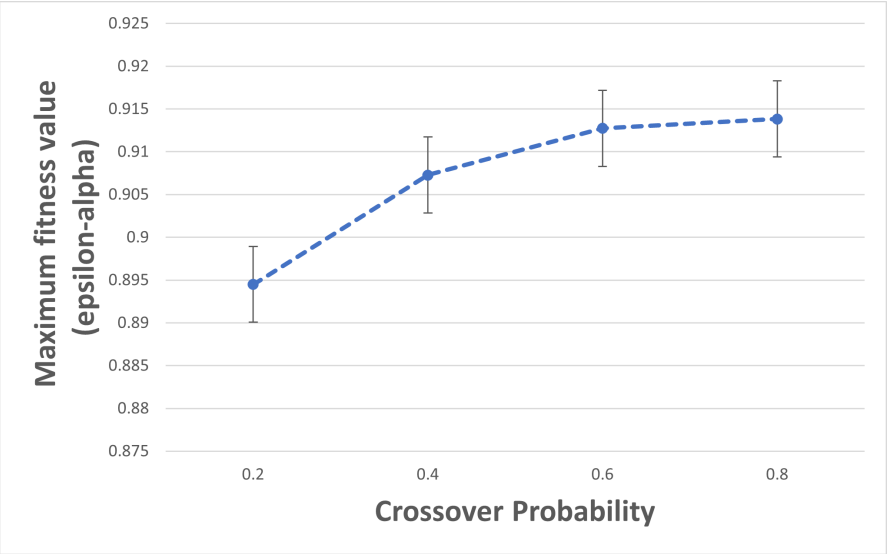

FIGURE 4.4: Maximum fitness value after 50 generations. Maximum fitness values are averaged after repeating the tests for five cycles to take into account of the random nature of GA. The error bars represent the standard deviation of each data point. Crossover rate of 0.8 is identified as the optimal rate and will be used in all following simulations.

4.3.3 Simulation results of mutation rate parameter

Applying the same methodology used for identifying the optimal crossover probability, Figure 4.5 below the results of mutation probability's effect on the average fitness values. The main difference when searching for the optimal mutation probability compared to the search for the optimal crossover probability is the assumption that the author should focus on lower mutation probabilities from the beginning. This assumption is based on G. Ochoa et al.'s study, which stated that a sufficiently small and fixed mutation rate should be implemented for optimal results [16]. The exact definition of what qualifies as sufficiently small is not clear and application-dependent but G. Ochoa et al. studied mutation rates between 0.001 to 0.01 so the author has used this range as a reference point. Due to the application-dependent nature of GA, another reference point used is M. Kim et al.'s use of 0.2 as its mutation rate in their recent radiative cooling GA study [8].

As shown in Figure 4.5's average fitness value versus number of generations plot, the author chose to analyse the mutation probabilities of 0.01, 0.02, 0.05, 0.1 and 0.2. Similar to the crossover probability analysis section, all curves follow the standard rotated-L shape with a high increase of average fitness value initially until around the 7^{th} to 9^{th} generation. However, the fact that all five curves plateau at

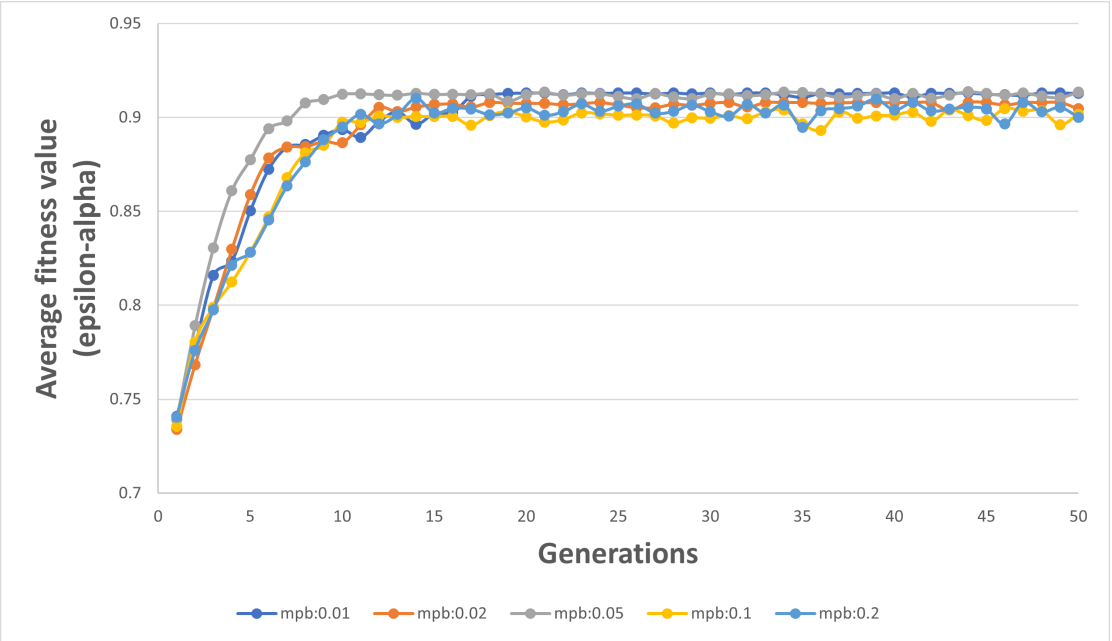

FIGURE 4.5: Comparison of different mutation probabilities (mpb): Average fitness value versus number of generations. Average fitness values are averaged after repeating the tests for five cycles. All five curves plateau at a very similar level and oscillate in a narrow range of approximately between 0.89 to 0.91 highlights the similarity in performance of this range of mutation rates. Thus, more evidence is needed to distinguish performance differences in mutation rates.

a very similar level and oscillate in a narrow range of approximately between 0.89 to 0.91 highlights the similarity in performance of this range of mutation rates.

This similarity shown by all five curves overlapping each other over 50 generations is expected as the analysis for mutation rates focuses on a much narrower range compared to the crossover rate analysis. That being said, the lack of significant difference in performance shown in Figure 4.5 means that the author needs another way to analyse the performances of different mutation rates.

This leads to Figure 4.6, where the author investigates the difference in performances of mutation probabilities by analysing maximum fitness values after fifty generations. Although this same methodology worked well in the crossover probability analysis, no concrete conclusion can be made with Figure 4.6's maximum fitness value versus mutation probability plot. This is because as the mutation rate increases, the average maximum fitness values fluctuate significantly without a clear trend. This fluctuation leads to the author's hypothesis of the performance effect of the initial population is greater than the effect of the mutation rate. To clarify, the initial population of each simulation is generated randomly and set as generation zero in the Python script.

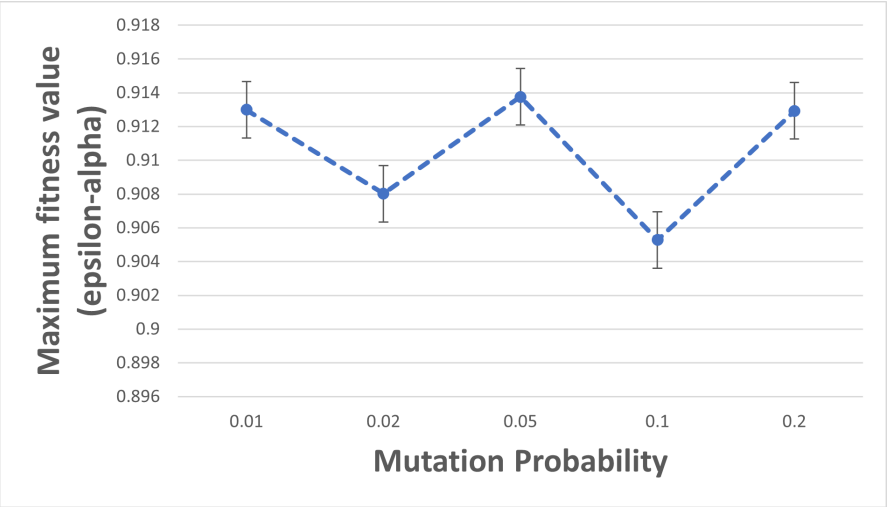

FIGURE 4.6: Difference in performances of mutation probabilities: Maximum fitness values after fifty generations. Maximum fitness values are averaged after repeating the tests for five cycles. The error bars represent the standard deviation of each data point. As mutation rate increases, the average maximum fitness values fluctuate significantly without a clear trend. This lack of differentiation in performances leads to the Fixed initial population tests in the next section.

Therefore, this hypothesis lead to an idea of fixing the initial population when testing all mutation probabilities. The testing of the hypothesis by implementing the fixed initial population method will be discussed in the following section.

4.3.3.1 Fixed initial population method

The core idea behind the fixed initial population method is that due to GA's inherent random nature, analysing mutation probabilities with the same starting population could generate insights that previous methods miss. The initial population used was arbitrary to prevent introducing bias to the tests. It was saved in a '.json' type file where the Python script could easily read simple data structures i.e. lists of materials and their corresponding thicknesses. Other than this change in using the same starting population for analysing all mutation rates, the methodology for testing remains the same including the important factor of having five test cycles.

Figure 4.7 shows the results of mutation probability's effect on average fitness values over 50 generations by plotting average fitness values against the number of generations. Importantly, the curves from Figure 4.5 where the tests didn't rely on a fixed initial population are far more similar with each other shown by a large

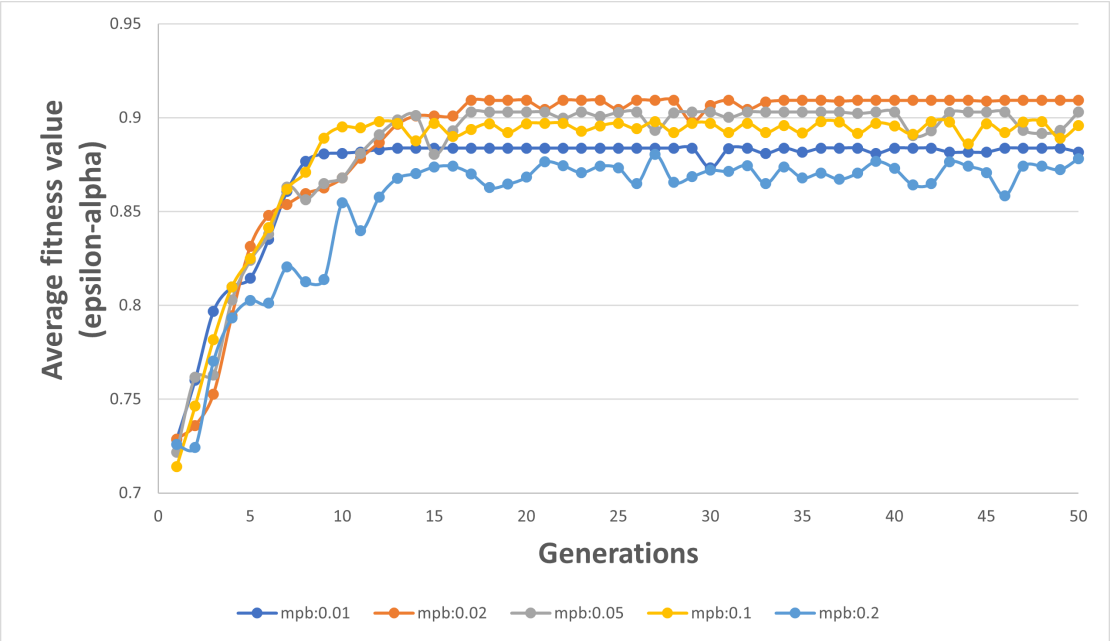

FIGURE 4.7: Fixed initial population test: Investigation of mutation probability's (mpb) effect on average fitness values over 50 generations. Average fitness values are the averages of five cycles. The curves of mutation probabilities 0.01 and 0.2 (the dark blue and light blue curve respectively) perform slightly poorer than the rest of mutation probabilities as these two curves oscillate at notably lower plateau levels. However, to verify this finding and to differentiate the performances of other mutation rates, an analysis using maximum fitness values is needed.

of amount of overlapping between the curves. The increase in differentiation of the curves in Figure 4.7 highlights the improvement caused by this alteration in methodology. It is clear that the curves of mutation probabilities 0.01 and 0.2 (the dark blue and light blue curve respectively) perform slightly poorer than the rest of mutation probabilities as these two curves oscillate at notably lower plateau levels.

However, to verify this finding and to differentiate the performances of other mutation rates, an analysis using maximum fitness values is needed. Before moving on to this next type of test, a clarification is required of why the average fitness values for the first generation are slightly different for different mutation rates. The starting population is initialised at generation zero, meaning that at generation one, one cycle of crossover and mutation has already occurred. Hence, the expectation of all data points starting at the exact same point for generation one for all mutation rates is not shown in Figure 4.7.

Figure 4.8 shows the mutation probability's effect on maximum fitness values by

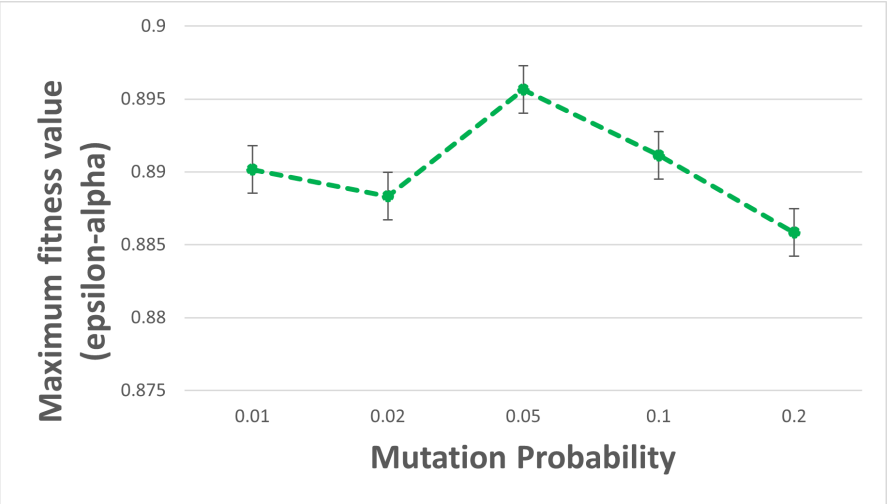

FIGURE 4.8: Mutation probability's effect on maximum fitness values: plotting maximum fitness values against mutation probability. Maximum fitness values are the averages of five cycles. The error bars represent the standard deviation of each data point. The mutation probability of 0.05 is selected as it has the highest maximum fitness value averaged over five test cycles. Hence, this mutation rate will be used in all remaining simulations.

plotting maximum fitness values against mutation probability. The curve underlines how similar the different mutation probabilities perform as all five data points lie between the range of 0.885 to 0.9. Unlike the analysis of crossover probabilities where the optimal one could be identified with relative ease, the mutation rates between 0.01 and 0.2 all perform very similarly.

However, to perform further tests such as comparing performances between using the $\epsilon - \alpha$ and $\epsilon \div \alpha$ fitness functions, a single optimal mutation probability needs to be chosen. Therefore, the mutation probability of 0.05 is selected as it has the highest maximum fitness value averaged over five test cycles. This mutation rate will be used in all remaining tests.

4.4 Tournament selection mechanism parameter

4.4.1 Introduction

Although there are many different selection mechanisms, there are no rules of thumb on which mechanism is better suited on a particular problem. However, the widely studied tournament selection mechanism is simple to implement. There

are several reasons why this is the case. Firstly, tournament selection only has a single control parameter - tournament size, which is typically denoted by 'k' [19]. In addition, this selection technique is scaling and translation invariant [20]. This means that the behaviour of the selection mechanism is not affected by the translation or scaling of the fitness values. As a result, unlike other mechanisms such as proportional selection, scaling methods are not required for tournament selection. For reasons mentioned above, this is the type of mechanism used in this project.

Before analysing the parameters associated with tournament selection, a term needs to be introduced. Selection pressure is defined as the strength of the selection mechanism [16]. This is measured by the ratio of maximum to average fitness values in a given population.

Tournament selection works by placing a higher weight to individuals that have higher fitness values. Thus, the probability of an individual to be selected for reproduction increases as its fitness value increases. The larger the tournament size, the higher the selection pressure as there are more competitors.

The most common k value used is 2, also known as binary tournament selection. Importantly, Y. Lavinas et al. stated that there is negligible justification of using this k value even though most researchers in the past 15 years have done so [19].

A recent study by M. Kim et al. consisted of using binary tournament selection [8]. The reason for this choice was not clear in the study other than stating that k = 2 is the default setting for the GA toolbox that they were using in MATLAB. Thus, it is a reasonable assume that the researchers did not analyse in detail about what might be the best k value to use.

Therefore, the primary purpose for the following section is to investigate this parameter in more depth than the typical radiative cooling optimisation study.

4.4.2 Results

Firstly, Figure 4.9 shows the significant improvement in average fitness values between k=1 (dark blue curve) and k=2 (orange curve). The dark blue curve oscillates below the 0.7 average fitness value level while the orange curve oscillates above the 0.85 level from approximately the 20^{th} generation onward. This highlights why binary tournament selection is such a popular default choice for many

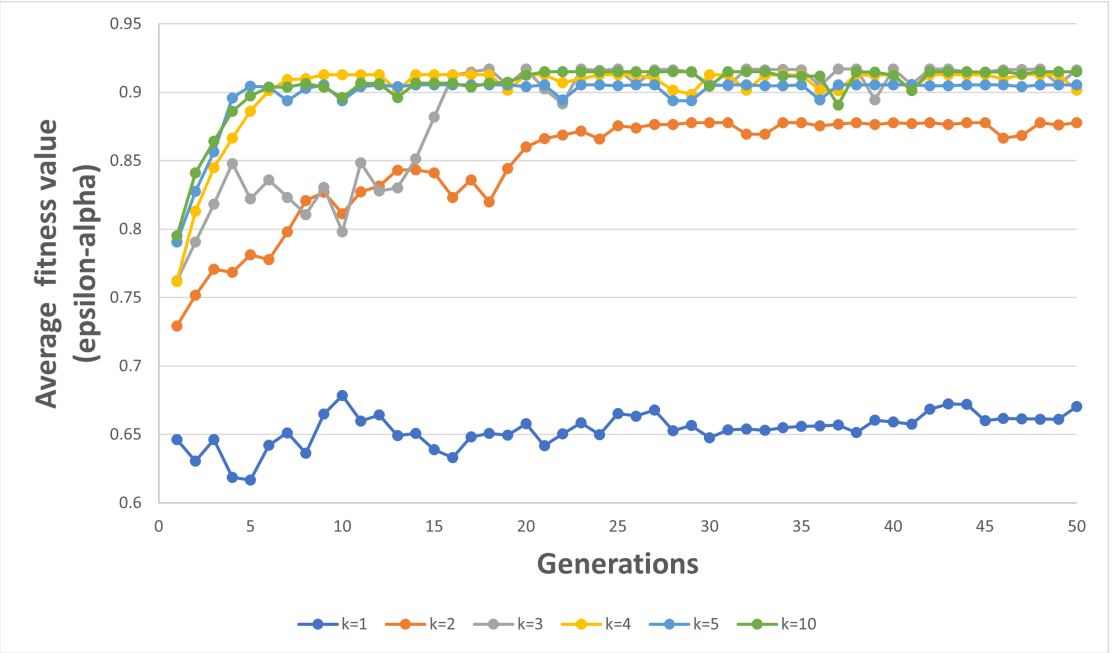

FIGURE 4.9: Tournament size's effect on average fitness values: Average fitness values against number of generations. Average fitness values are the averages of five test cycles. The performances of k=3,4,5 and 10 are significantly better than lower k values. However, these four curves of higher k values behave very similarly after the k=3 curve reaches the 0.9 level at the 16^{th} generation. Thus, further analysis is needed with the help of another plot.

researchers when using GAs for optimisation problems [19]. That being said, it is important to investigate whether even higher k values might work better in this project's specific application.

The four other curves (i.e. representing k=3, 4, 5 and 10.) all oscillate at an even higher level than the k=2 curve, at around the 0.9 average fitness value level. The k=3 (grey) curve needed more time to reach the 0.9 level compared to k=4, 5 and 10, shown by the the grey curve's initial lower oscillation level between 0.8 and 0.85 level from around the 3^{rd} generation until the 13^{th} generation. This matches with the theory that as the tournament size increases, the convergence speed typically increases. This is because a lower k value like k=3, gives a higher probability for the rest of the individuals to be selected for the crossover stage, which preserves genetic diversity.

Despite this difference, these four curves behave very similarly after the k=3 curve reaches the 0.9 level at the 16^{th} generation. Thus, further analysis is needed with the help of another plot.

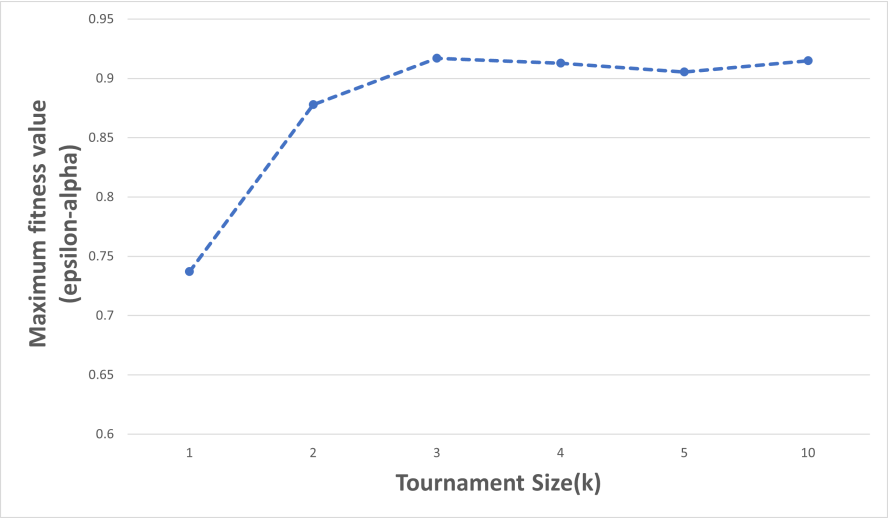

FIGURE 4.10: Tournament size's effect on maximum fitness values: Maximum fitness values against tournament size (k). Maximum fitness values are the averages of five test cycles. The k value of 3 is identified as the optimal tournament size. Thus, this tournament size will be used in all following simulations.

Figure 4.10 helps with differentiating the performance differences in k=3,4,5 and 10. This figure consists of plotting maximum fitness values against tournament size. Similar to previous tests, the maximum fitness values are averaged over five test cycles. Figure 4.10 highlights that even though the largest increase in performance is between k=1 and k=2, there is an additional boost in performance when k is increased beyond the value of 2. The maximum fitness value reached by k=3,4,5 and 10 are close but the k=3 test achieved the highest fitness value of 0.91706.

Note that all tests prior to the investigation in tournament size in this section, were coincidentally set as k=3. The implementation of the optimal k parameter is accidental, but this accidental selection increases the validity of the results obtained as different k values could behave differently with different combinations of parameters.

The explanation of the performance increase between k=2 and k=3 is that the increase in tournament size leads to an increase in the selection pressure due to the presence of additional competitors. However, the performance decrease when k is larger than 3 could be due to the decrease in genetic diversity. The increase in tournament size causes weak individuals to have lower probabilities to be selected for crossover.

The limitation of the results obtained is that the difference of maximum fitness values is very small in magnitude. The percentage difference in the maximum fitness value obtained by k=3,4,5 and 10 is all within 1.5%. Furthermore, if the results match perfectly with theory, the maximum fitness value would decrease consistently as the k increases. However, this is not the case in reality. Even though the maximum fitness value decreases consistently as k increases from k=3 to k=5, the maximum fitness value obtained when k=10 is the second highest (behind k=3).

4.5 Comparison between fitness functions

This section compares the performances between $\epsilon - \alpha$ and $\epsilon \div \alpha$ fitness functions. The methodology used is different to tests done previously. Firstly, the optimal crossover and mutation rates found using the $\epsilon - \alpha$ fitness function is applied to the test script with the $\epsilon \div \alpha$ fitness function. Then, the comparison involves plotting emissivity versus wavelength graphs of the best multilayer structures produced by GA for each fitness function. The variable of net cooling power of the multilayer structures will be used in the comparison as well.

The change in methodology to utilising spectral plots and net cooling power values is because these are the factors that are ultimately relevant when designing a radiative cooler. The net cooling power equation is shown in Equation 2.1. Note that WPtherml's net cooling power calculations do not take convection and conduction into account.

TABLE 4.1: Performance comparison of $\epsilon - \alpha$ and $\epsilon \div \alpha$ fitness functions. The ϵ and α values are averaged over five tests for each fitness function. When the $\epsilon \div \alpha$ fitness function is used, GA places a higher weight to α as expected in theory due to the non-linear relation between ϵ and α. This is shown by the relatively high percentage difference of 12.6% for the α values. However, the low percentage difference of 0.91% for the ϵ values do not match with the theory that using the $\epsilon \div \alpha$ fitness function would place significantly less emphasis on maximising the ϵ value.

Fitness function	Average ε	Average α
ε-α	0.93956	0.03002
ε/α	0.93102	0.02646
% Difference	0.91%	12.6%

Similar to previous tests, five tests were run for both fitness functions. Table 4.1 is used to further compare the behaviour of GA relying on different fitness functions. In theory, the GA based on the $\epsilon \div \alpha$ fitness function should exhibit the behaviour of placing a heavier weight on the objective of minimising α due to the non-linear relation between ϵ and α. Table 4.1 indeed highlights GA giving a higher weight to α, shown by the relatively high percentage difference of 12.6% for the α values.

However, the very low percentage difference of 0.91% for the average ϵ values do not match with the theory that using the $\epsilon \div \alpha$ fitness function would place significantly less emphasis on maximising ϵ. The hypothesis is that the use of $\epsilon \div \alpha$ fitness function would lead to significantly lower average ϵ value compared to the use of the $\epsilon - \alpha$ fitness function. This hypothesis leads to the expectation that the spectral plot from the $\epsilon \div \alpha$ fitness function would have a lower curve within the 8 to 13 μm wavelength range. The following analysis explores how valid this hypothesis is in practice.

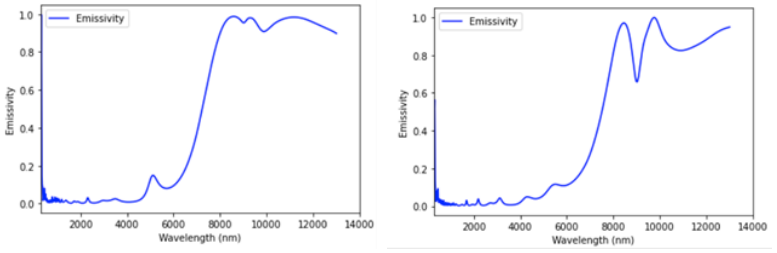

FIGURE 4.11: (Left) Spectral plot from $\epsilon - \alpha$ fitness function, the best individual achieved the highest fitness value of 0.926; (Right) Spectral plot from $\epsilon \div \alpha$ fitness function, the best individual achieved the highest fitness value of 30.82. The best multilayer structures were selected after five tests based on the highest fitness value for the respective fitness function.

For each fitness function, the best multilayer structure was selected after five tests based on the highest fitness value for the respective fitness function. Specifically, the spectral plot on the left in Figure 4.11 is from the individual which achieved the highest fitness value of 0.926 from the $\epsilon - \alpha$ fitness function. Specifically, this individual's structure (excluding its reflective Silver base layer which is held constant in all tests) is $Al_2O_3, SiO_2, Si_3N_4, CaF_2$ (from top to bottom layer) with its corresponding thicknesses being 1.04 μm, 0.36 μm, 1.45 μm and 0.3μm. While the spectral plot on the right is derived from the individual which achieved the highest fitness value of 30.82 from the $\epsilon \div \alpha$ fitness function. This individual consists of the same materials in the same order as the previously mentioned individual but its corresponding thicknesses are 1.69 μm, 0.38 μm, 0.14 μm and 0.16μm.

The most important observation from Figure 4.11 is that the left-hand side plot underlines that the $\epsilon - \alpha$ fitness function places a heavy weight for the objective of maximising the emissivity value across the entire ϵ range (8-13 μm). This is highlighted by the relatively smooth curve that has consistently high emissivity values in the 8-13 μm window. Conversely, the spectral plot on the right emphasises the smaller weight placed on the objective of maximising the ϵ value by the $\epsilon \div \alpha$ fitness function. This is underscored by the fluctuating M-shaped emissivity curve that has a significant drop in emissivity between approximately 8 μm to 9 μm.

The limitation of this finding is that despite the existence of this fluctuating M-shaped emissivity curve, this curve does not perfectly match the hypothesis because the expectation was that the curve between the entire ϵ range would be shifted to an even lower emissivity level. The M-shaped curve shows that even with using the $\epsilon \div \alpha$ fitness function, it reaches higher than expected emissivity level, highlighted by the high peaks of the M-shaped curve.

Due to the minute α values, it is challenging to draw any concrete conclusions with Figure 4.11 for the contrast in emphasis placed on the α variable by the two fitness functions. However, the comparison of α values has been explained well by Table 4.1. and its subsequent analysis. Nevertheless, additional evidence is needed to improve the validity of the performance comparison of the fitness functions.

Figure 4.12 has two data sets shown by the left y-axis representing the values of $\epsilon - \alpha$ fitness function and the other y-axis on the right representing the values of $\epsilon \div \alpha$ fitness function, for which both are plotted against net cooling power. This plot shows that there is a clear direct proportional relationship between $\epsilon - \alpha$ values and the net cooling power values. However, the nearly horizontal trend line that represents the relationship between $\epsilon \div \alpha$ values and the net cooling power values emphasises the lack of differentiation between fitness values and net cooling power values. This highlights the ineffectiveness of using $\epsilon \div \alpha$ as GA's fitness function.

Table 4.2 shows the test results based on the $\epsilon \div \alpha$ fitness function (*denotes the original fitness function used in the tests). This fitness function is the original metric used to obtain the best individual i.e. the individual from Test 4 with the fitness value of 30.82. However, the 3^{rd} column shows that by using the same ϵ and α values to re-calculate fitness values based on the other fitness function, $\epsilon - \alpha$, a more detailed comparison can be made. In addition to comparing both fitness functions, components needed to calculate the net cooling power (i.e. radiative

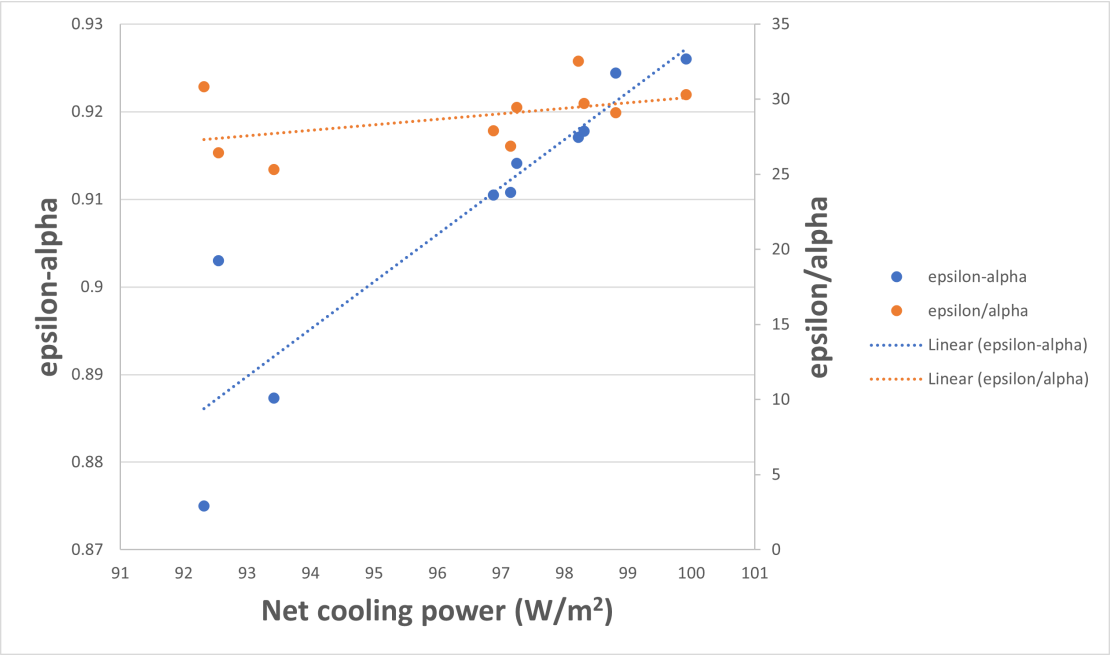

FIGURE 4.12: Comparison of effectiveness of fitness functions: The left y-axis represents the values of $\epsilon - \alpha$ fitness function and the right y-axis represents the values of $\epsilon \div \alpha$ fitness function, for which both are plotted against net cooling power. There is clear direct proportional relationship between $\epsilon - \alpha$ values and the net cooling power values. However, the nearly horizontal trend line that represents the relationship between $\epsilon \div \alpha$ values and the net cooling power values emphasises the lack of differentiation between fitness values and net cooling power values. This highlights the ineffectiveness of using $\epsilon \div \alpha$ as GA's fitness function.

power, solar warming power, atmospheric power) are included in the table, alongside the 7^{th} column representing the net cooling power. To ensure conciseness of the table display, the three most important criteria (i.e. $\epsilon \div \alpha$, $\epsilon - \alpha$ and net cooling power) are denoted by a numeric value in brackets which correspond to the three rank columns on the right side of the table. This table lacks the structures and the thicknesses of the radiative coolers as the comparison focuses on the results of different fitness functions. However, the complete results are included in Appendix (A.1).

Importantly, Table 4.2 shows that there is a perfect match between the Rank (2) and Rank (3) columns. This highlights that $\epsilon - \alpha$ fitness function outperforms the $\epsilon \div \alpha$ function as it suggests that fitness values derived from $\epsilon - \alpha$ give a better indication for their resultant net cooling power values. Moreover, the significantly poorer performance of the $\epsilon \div \alpha$ function is underlined by the Rank (1)'s column assignment of 4 for the individual with the highest net cooling power.

TABLE 4.2: Test results based on the $\epsilon \div \alpha$ fitness function. (*denotes the original fitness function used in the tests, while other criteria are added for an in-depth comparison.) Each of the three criteria are denoted by a numeric value in brackets which corresponds to the three rank columns on the right side of the table. There is a perfect match between the Rank (2) and Rank (3) columns. This highlights that $\epsilon - \alpha$ fitness function clearly outperforms the $\epsilon \div \alpha$ function. Moreover, the significantly poorer performance of the $\epsilon \div \alpha$ function is underlined by the Rank (1)'s column assignment of 4 for the individual with the highest net cooling power.

Test No.	*ε/α (1)	ε-α (2)	Radiative Power (W/m^2)	Solar warming power (W/m^2)	Atmospheric warming power (W/m^2)	Net cooling power (W/m^2) (3)	Rank (1)	Rank (2)	Rank (3)
1	29.45	0.9141	158.1	20.02	40.83	97.25	3	3	3
2	26.86	0.9108	158.9	20.44	41.33	97.15	5	4	4
3	29.71	0.9178	159.2	20.20	40.66	98.31	2	2	2
4	30.82	0.8750	147.9	19.82	35.72	92.32	1	5	5
5	29.10	0.9244	154.7	20.88	34.99	98.81	4	1	1

As a result, the conclusion from this test cycle is that $\epsilon - \alpha$ performs better than $\epsilon \div \alpha$. The poor performance of $\epsilon \div \alpha$ compared to $\epsilon - \alpha$ is best explained by Figure 4.12, but the precise reason why $\epsilon \div \alpha$ still generates individuals with very high net cooling power is not clear. However, a hypothesis is that the very limited pool of four materials which are all known to be excellent materials in the radiative cooling application leads to the generation of universally high net cooling power individuals. Therefore, in future research, this bias of including only good-performing materials could be removed by randomly adding other materials that are not known to be high performers in the radiative cooling application. This part of research is outside of the scope for this project.

The above analysis based on Table 4.2 only covers the cycle of $\epsilon \div \alpha$ tests. Thus, including Table 4.3 ensures that the analysis is complete and unbiased.

The methodology used and the order of the variables in Table 4.3 is identical to Table 4.2 for ease of understanding, but note that the * denotation is on the 3^{rd}

TABLE 4.3: Test results based on the $\epsilon - \alpha$ fitness function. (*denotes the original fitness function used in the tests, while other criteria are added for an in-depth comparison.) Each of the three criteria are denoted by a numeric value in brackets which corresponds to the three rank columns on the right side of the table. The $\epsilon - \alpha$ fitness function ranked the 4^{th} test as the best individual which matches with the rank of net cooling power. While the $\epsilon \div \alpha$ fitness function is less effective as it ranked the individual with the highest net cooling power as the second-best individual. The limitation from this table is that despite the $\epsilon - \alpha$ fitness function being able to identify the best individual, its ranking is not perfect as shown by the mismatch between the 4^{th} and 5^{th} ranks in the Rank (2) and Rank (3) column.

Test No.	ε/α (1)	* ε-α (2)	Radiative Power (W/m^2)	Solar warming power (W/m^2)	Atmospheric warming power (W/m^2)	Net cooling power (W/m^2) (3)	Rank (1)	Rank (2)	Rank (3)
1	32.53	0.9171	151.3	18.35	34.71	98.22	1	2	2
2	27.91	0.9105	157.7	20.03	40.77	96.88	3	3	3
3	26.44	0.9030	156.1	22.03	41.49	92.55	4	4	5
4	30.31	0.926	159.6	20.09	39.59	99.92	2	1	1
5	25.32	0.8873	157.0	23.31	40.22	93.42	5	5	4

column as this cycle of test results are derived from the $\epsilon - \alpha$ fitness function.

Firstly, the $\epsilon - \alpha$ fitness function ranked the 4^{th} test as the best individual which matches with the rank of net cooling power. While the $\epsilon \div \alpha$ fitness function is less effective as it ranked the individual with the highest net cooling power as the second-best individual. The limitation from this table is that despite the $\epsilon - \alpha$ fitness function being able to identify the best individual, its ranking is not perfect as shown by the mismatch between the 4^{th} and 5^{th} ranks in the Rank (2) and Rank (3) columns.

4.6 Tests on scaling up program

4.6.1 Introduction

Prior to this section, all tests were done with four candidate materials. Though many insights on optimal parameters have been found, testing the program that it could scale up properly is an important step towards building a program that could be useful to researchers. Thus, increasing the candidate pool size to six and eight will be explored.

The methodology involved is more simple than previous sections' tests as analysis prior to this section already form the bulk of this project. This section's objective is to verify that the software built is capable of supporting larger candidate pools. To achieve this objective, common materials used in recent radiative cooling research papers are added to the existing candidate pool of four materials used in previous tests. As with the author's justification of the materials chosen to form the initial candidate pool, the fundamental criteria is that there is n-k data that covers sufficient wavelengths from reputable academic papers. These n-k data of added materials comes from 'refractiveindex.info'[12].

Similar to Section 4.5, the methodology in this section consists of running five tests for each pool size and identifying the best structure based on the $\epsilon - \alpha$ fitness function while displaying the best individual's spectral plot.

4.6.2 Results from candidate pool size of 6 and 8

For testing the scale up to 6 materials, Titanium dioxide and Hafnium dioxide were added to the original four materials in the candidate pool. Therefore, the resulting pool for this cycle test is - $CaF_2, Al_2O_3, Si_3N_4, SiO_2, TiO_2$ and HfO_2. As with all previous tests, the material of Silver and its thickness is fixed as the reflective base layer.

Figure 4.13 displays the spectral plot of the fittest individual in candidate pool size of 6 tests. This structure achieved a net cooling power of 88.61 W/m^2.

For testing the scale up to 8 materials, the new candidate pool is formed by adding Silicon carbide and Magnesium fluoride to the six materials mentioned.

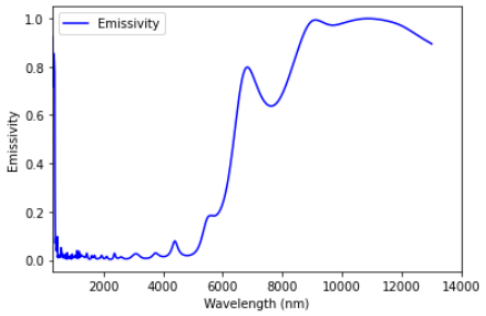

FIGURE 4.13: Spectral plot of the best individual in candidate pool size of 6 tests. Structure (top to bottom layer): $CaF_2, TiO_2, HfO_2, Al_2O_3, Si_3N_4$ and SiO_2. The corresponding thicknesses are: 1.60 μm, 1.11 μm, 0.77 μm, 0.35 μm, 1.97 μm and 0.39 μm. This structure achieved a net cooling power of 88.61 W/m^2.

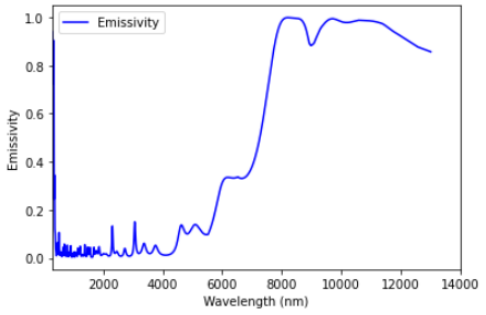

FIGURE 4.14: Spectral plot of the fittest individual in candidate pool size of 8 tests. Structure (top to bottom layer): $Al_2O_3, SiC, CaF_2, MgF_2, HfO_2, SiO_2$, Si_3N_4 and TiO_2. The corresponding thicknesses are: 0.88 μm, 1.51 μm, 1.99 μm, 0 μm, 0.88 μm, 0.51 μm, 1.46 μm and 0.16 μm. This structure achieved a net cooling power of 79.81 W/m^2.

Figure 4.14 displays the spectral plot of the fittest individual in candidate pool size of 8 tests. This structure achieved a net cooling power of 79.81 W/m^2. Note that the algorithm set the 4^{th} layer's thickness to be 0 μm, so MgF_2 is not used for this individual.

4.6.3 Conclusion of scale up section

Table 4.4 gives a summary of the fittest individuals obtained via different sizes of candidate material pools. In this test, n=4 produced the individual with the highest net cooling power. However, this is not the purpose of this test nor an important takeaway of the project. The important learning point is that this table shows that the increase in the size of candidate pool does not necessarily mean that

TABLE 4.4: Summary table of the fittest individuals obtained via different sizes of candidate material pools. (*denotes that the original fitness function used in the tests is $\epsilon - \alpha$). The structure of the table is very similar to previous tables in the Comparison of fitness function section. The main different is the first column which has 'n' representing the candidate material pool size. Five tests were run for each candidate material pool size, with the fittest individual selected based on its $\epsilon - \alpha$ value. This table shows that the increase in the size of candidate pool does not necessarily mean that the individuals generated by GA are more likely to achieve a higher net cooling power. These results align with M. Kim et al.'s study finding that although the researchers included ten materials in its candidate pool, the optimised eight-layer individual composed of only three materials - Al_2O_3, SiO_2 and Si_3N_4.

Best individual from material pool size n	ε/α	*ε-α	Net cooling power (W/m^2)
n = 4	30.31	0.9260	99.92
n = 6	21.13	0.9091	88.61
n = 8	18.17	0.8988	79.81

the individuals generated by GA are more likely to achieve a higher net cooling power. These results align with M. Kim et al.'s study finding that although the researchers included ten materials in its candidate pool (as mentioned in Section 2.2), the optimised eight-layer individual composed of only three materials - Al_2O_3, SiO_2 and Si_3N_4 (excluding the Silver reflective base layer) [8].

To conclude, the author suggests that researchers should consider using net cooling power as the GA's fitness function because this is the most relevant factor for radiative cooler designers. As an example, M. Kim et al.'s 2021 optimisation of radiative cooler study used net cooling power as the GA's fitness function [8]. If computing net cooling power in GA or other types ML models require too much computational power and hence excessive run time, using the $\epsilon - \alpha$ fitness function is a good choice.

Chapter 5

Evaluation and Conclusion

5.1 Project Management

Project management consisted of planning tasks that need to be completed to achieve the overall project goals in time and understanding what approach is best to complete them. Agile methodology was used as this iterative form of project management enabled the author to build a minimum viable product (i.e. a simplified version of GA with limited materials and fixed thicknesses) in Semester 1 while spending Semester 2 developing a complete Python script which incrementally supported 4, 6 and finally 8 materials.

The development of Gantt charts and a risk assessment table assisted the planning process. Two Gantt charts are shown in Appendix B.1 and as shown in Table 5.1., project risk was measured by multiplying the loss variable by the probability.

These two tools were useful and served as a general guide but the most important action in relation to time management was the Powerpoint slides the author made for the weekly supervisor meetings. This form of documenting weekly progress was a great way to stay on schedule and identifying problems proactively.

Another proactive decision which drastically mitigated the risk of lacking the requisite programming skills (as mentioned in Table 5.1), was the author's decision to study the Machine Learning Technologies module in Semester 1. This additional practical ML experience enabled this project to be completed on time.

TABLE 5.1: Risk assessment table: A scale of 5 (1 for the lowest and 5 for the highest) is used to assign the likelihood of a problem occurring and to assign the severity of damage caused by the problem if it did occur. Project risk is measured by multiplying the loss variable by the probability.

Problem	**Loss** (Severity of damage caused by the issue)	**Probability** (Likelihood of issue occurring)	**Risk** (Loss x Probability)	**Solution** (Counteracting policy against problem)
Loss of project files	5	1	5	Back up all files on ECS H drive.
Lacking the requisite skillset for programming genetic algorithm	2	5	10	Allow more time in designing and implementing ML models.
Lack of n-k data that covers the full wavelength range	1	5	5	Only use materials that have sufficient n-k data.
Contracting Covid	4	4	16	Wear mask as often as possible.
Using programming packages that are not suitable for project's goals.	4	2	8	Allow more time to choose appropriate software packages.

5.2 Evaluation and future work

A limitation of this project is the selection mechanism investigation. The single control parameter of the tournament selection mechanism ensured that the project scope did not increase excessively. However, as there are many more selection mechanisms that have the potential to improve the effectiveness of the GA, researchers should consider at least several other mechanisms. Several popular selection mechanisms include the Roulette selection, Non-dominated Sorting selection and Strength Pareto selection mechanisms. All three mechanisms mentioned are supported by existing built-in functions in the DEAP package. Similarly, all tests were run with an arbitrarily set 2-point crossover mechanism. Thus, further research should include exploring the wide range of other crossover mechanisms.

An important limitation is that the author was not able to fully integrate the net cooling power fitness function into the GA comparison due to the delayed release of a WPtherml package update. M. Kecebas et al. stated that focusing on the optimisation via the net cooling power of a radiative cooler may lead to better results compared to optimising its spectral response [21]. Hence, it would have

been ideal to conduct a full investigation in the performance of GA based on using net cooling power as the fitness function in addition to the current completed comparison of $\epsilon \div \alpha$ and $\epsilon - \alpha$ fitness functions. Also, as shown in equation (2.1) in Section 2.1, conduction and convection heat transfer are part of the net cooling power calculation. Thus, a limitation of the net cooling power values obtained in this project's simulations is that conduction and convection are not taken into account.

However, the author is grateful to have received the unreleased beta version of the update from WPtherml developers in late April. This enabled the inclusion of the investigation in the performances of $\epsilon \div \alpha$ and $\epsilon - \alpha$ based on the corresponding net cooling power values in Section 4.5.

5.3 Conclusion

To conclude, the author has successful created a fully working model that could optimise radiative coolers using GA and thoroughly investigated the effects of GA parameters in more depth than the typical radiative cooling optimisation study. Specifically, the optimal crossover and mutation probabilities are found to be 0.8 and 0.05 respectively, with the optimal tournament size being 3.

This project tested the software up to supporting eight commonly used materials in recent literature but the number of materials could increase with simple changes to the data library files. Furthermore, although this project focused on GA based on $\epsilon \div \alpha$ and $\epsilon - \alpha$ fitness functions, with the latter found to perform better, the software built can support any fitness function.

In terms of the novelty of this project, there are several recent academic papers that utilise GA to optimise radiative coolers, with most if not all of them cited in this report. Many of these studies use MATLAB and reading papers such as M. Kim et al. which consisted of using binary tournament selection without any justification apart from stating that it was the default setting in MATLAB, suggests that there is a strong argument for researchers to explore using other potentially more flexible software packages [8]. In this sense, this project is novel because from the author's communications with WPtherml developers, it is clear that they have not heard of the DEAP GA package. Thus, it is the first time that the WPtherml package was utilised in conjunction with the DEAP package.

The author hopes that this project enables researchers to utilise the values of GA parameters used in the investigation as reference points and could make them feel confident that it is a good option to consider using WPtherml combined with DEAP when optimising radiative coolers.

Bibliography

[1] "State of Climate in 2021: Extreme events and major impacts," Oct. 2021. [Online]. Available: https://public.wmo.int/en/media/press-release/state-of-climate-2021-extreme-events-and-major-impacts

[2] O. Deschênes and M. Greenstone, "Climate change, mortality, and adaptation: Evidence from annual fluctuations in weather in the us," *American Economic Journal: Applied Economics*, vol. 3, no. 4, pp. 152–85, 2011.

[3] A. Barreca *et al.*, "Adapting to climate change: The remarkable decline in the us temperature-mortality relationship over the twentieth century," *Journal of Political Economy*, vol. 124, no. 1, pp. 105–159, 2016.

[4] T. Abergel and C. Delmastro, "Tracking buildings 2021," 2020.

[5] A. P. Raman *et al.*, "Passive radiative cooling below ambient air temperature under direct sunlight," *Nature*, vol. 515, no. 7528, pp. 540–544, 2014.

[6] Y. Zhang *et al.*, "Photonics empowered passive radiative cooling," *Advanced Photonics Research*, vol. 2, no. 4, p. 2000106, 2021.

[7] B. Zhao *et al.*, "Radiative cooling: A review of fundamentals, materials, applications, and prospects," *Applied energy*, vol. 236, pp. 489–513, 2019.

[8] M. Kim *et al.*, "Optimization and performance analysis of a multilayer structure for daytime radiative cooling," *Journal of Quantitative Spectroscopy and Radiative Transfer*, vol. 260, p. 107475, 2021.

[9] D. Zhao *et al.*, "Radiative sky cooling: Fundamental principles, materials, and applications," *Applied Physics Reviews*, vol. 6, no. 2, p. 021306, 2019.

[10] P. You *et al.*, "High-performance multilayer radiative cooling films designed with flexible hybrid optimization strategy," *Materials*, vol. 13, no. 13, p. 2885, 2020.

[11] M. A. Zaman, "Photonic radiative cooler optimization using taguchi's method," *International Journal of Thermal Sciences*, vol. 144, pp. 21–26, 2019.

[12] M. Polyanskiy, "Refractiveindex.info," 2008. [Online]. Available: https://refractiveindex.info/

[13] J. F. Varner *et al.*, "Wptherml: A python package for the design of materials for harnessing heat," *Journal of open research software*, vol. 7, 2019.

[14] F.-A. Fortin *et al.*, "Deap: Evolutionary algorithms made easy," *The Journal of Machine Learning Research*, vol. 13, no. 1, pp. 2171–2175, 2012.

[15] Y. Huang *et al.*, "Broadband metamaterial as an "invisible" radiative cooling coat," *Optics Communications*, vol. 407, pp. 204–207, 2018.

[16] G. Ochoa, I. Harvey, and H. Buxton, "On recombination and optimal mutation rates," in *Proceedings of the genetic and evolutionary computation conference*, vol. 1. Citeseer, 1999, pp. 488–495.

[17] E. A. Williams and W. A. Crossley, "Empirically-derived population size and mutation rate guidelines for a genetic algorithm with uniform crossover," in *Soft computing in engineering design and manufacturing*. Springer, 1998, pp. 163–172.

[18] A. J. Umbarkar and P. D. Sheth, "Crossover operators in genetic algorithms: a review." *ICTACT journal on soft computing*, vol. 6, no. 1, 2015.

[19] Y. Lavinas *et al.*, "Experimental analysis of the tournament size on genetic algorithms," in *2018 IEEE International Conference on Systems, Man, and Cybernetics (SMC)*. IEEE, 2018, pp. 3647–3653.

[20] T. Blickle, "Tournament selection," *Evolutionary computation*, vol. 1, pp. 181–186, 2000.

[21] M. A. Kecebas *et al.*, "Spectrally selective filter design for passive radiative cooling," *JOSA B*, vol. 37, no. 4, pp. 1173–1182, 2020.

Appendix A

Results Tables

Test No.	Material (from top to bottom layers)	Thickness (um)	Epsilon/Alpha (1)	*Epsilon-Alpha (2)	P_rad	P_sun	P_atm	P_cool (3)	Rank (1)	Rank (2)	Rank (3)
1	Al2O3, SiO2, Si3N4, CaF2	1.53, 0.27, 0.61, 1.31	32.53	0.9171	151.3	18.35	34.71	98.22	1	2	2
2	Al2O3, SiO2, Si3N4, CaF2	0.86, 0.31, 1.68, 0.2	27.91	0.9105	157.7	20.03	40.77	96.88	3	3	3
3	Al2O3, Si3N4, SiO2, CaF2	0.93, 1.93, 1.15, 1.28	26.44	0.9030	156.1	22.03	41.49	92.55	4	4	5
4	Al2O3, SiO2, Si3N4, CaF2	1.04, 0.36, 1.45, 0.3	30.31	0.926	159.6	20.09	39.59	99.92	2	1	1
5	CaF2, Al2O3, SiO2, Si3N4	1.76, 0.85, 0.4,1.28	25.32	0.8873	157.0	23.31	40.22	93.42	5	5	4

Test No.	Material (from top to bottom layers)	Thickness (um)	*Epilson/Alpha (1)	Epsilon-Alpha (2)	P_rad	P_sun	P_atm	P_cool (3)	Rank (1)	Rank (2)	Rank (3)
1	Al2O3, Si3N4, SiO2, CaF2	1.13, 1.8,1.94,1.04	29.45	0.9141	158.1	20.02	40.83	97.25	3	3	3
2	Al2O3, Si3N4, SiO2, CaF2	1.16, 1.89, 1.33, 1.47	26.86	0.9108	158.9	20.44	41.33	97.15	5	4	4
3	Al2O3, SiO2, Si3N4, CaF2	0.98, 0.39, 1.36, 0.21	29.71	0.9178	159.2	20.20	40.66	98.31	2	2	2
4	Al2O3, SiO2, Si3N4, CaF2	1.69, 0.38, 1.4,0.16	30.82	0.8750	147.9	19.82	35.72	92.32	1	5	5
5	Al2O3, SiO2, Si3N4, CaF2	1.43, 0.34, 0.87, 1.05	29.10	0.9244	154.7	20.88	34.99	98.81	4	1	1

FIGURE A.1: Complete results for the Comparison between fitness functions section (including materials and corresponding thicknesses).

Appendix B

Gantt Charts

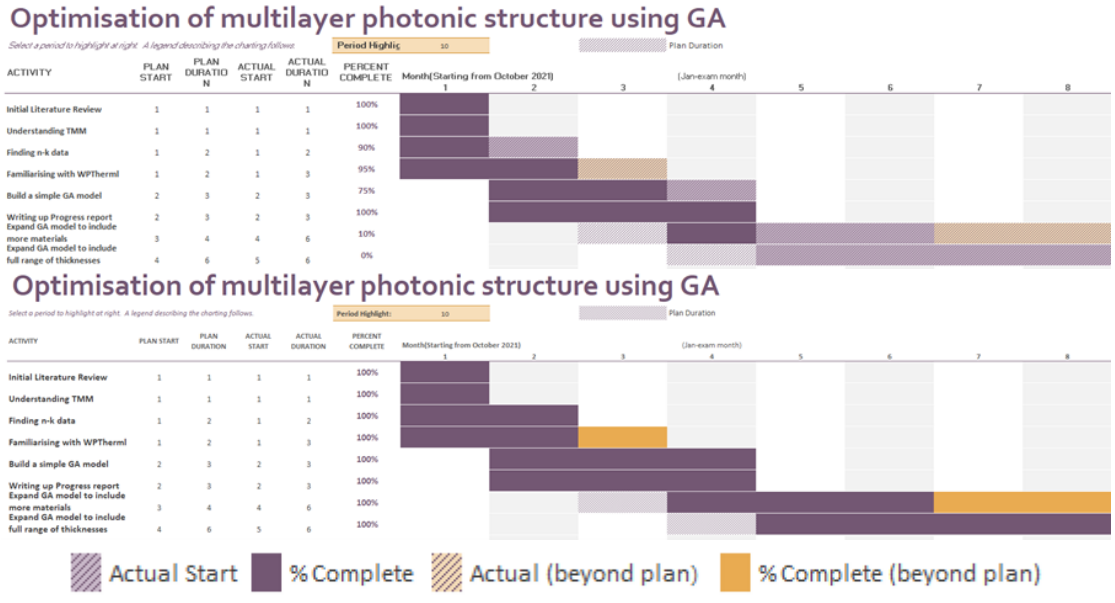

FIGURE B.1: (Top) Gantt chart for Semester 1; (Bottom) Gantt chart for Semester 2.

Appendix C

Project Brief

C.1 Problem

Radiative cooling technology has the potential to bring about significant impact on several industries, particularly in reducing energy consumption in buildings which makes up 40% of the total energy consumption of the world. Currently, large proportion of that energy is used for indoor thermal management via conventional HVAC systems. By utilising radiative cooling technology, a passive way of decreasing cooling energy requirements without additional power input could be realised. This technology involves a mechanism that passively obtains cooling energy by releasing heat of terrestrial-facing objects into the cold sink of outer space.

The development of photonic radiators and metamaterials has enabled significant technological advancements in innovative design and fabrication of radiators. The recent novel materials and structures of various radiators developed have created a new class of radiators – selective infrared radiators, which further highlights the advantages of diurnal radiative cooling.

C.2 Goals

Despite recent advancement in design and fabrication of selective infrared radiators, challenges remain which require further research. These challenges include but are not limited to understanding what materials and what structure are best

suited to incorporate into the multi-layered design of photonic radiators. Raman et al demonstrated a planar photonic radiator which comprises of seven alternating layers of hafnium dioxide and silica with varying thickness on top of 200 nm thick silver and 750µm thick silicon wafer substrate [1].

Currently, there is insufficient research on materials and structures which utilises machine learning techniques for advancing understanding of how to optimise parameters of photonic radiators. Hence, the primary goal of this project is to explore the potential of using evolutionary algorithms to enhance understanding of how to optimise the thickness and materials used in radiator design.

C.3 Scope

Firstly, calculating a thin-film spectrum is an important starting point. This can be achieved by using the transfer matrix which is a connection between refractive index and absorptivity. After understanding the transfer matrix and the related mathematical formulas, different ideal spectrum for various conditions should be considered.

Furthermore, after performing a literature review, a pool of materials and several design structures of photonic radiators should be chosen for integrating these two types of parameters into the genetic algorithm.

Lastly, in terms of the genetic algorithm, the creation of several fitness functions and consideration of hyper-parameters are needed. These parameters include but are not limited to the number of generations, the size of the population, cross-over and mutation probabilities.

[1] Raman AP, Anoma MA, Zhu L, Rephaeli E, Fan S. Passive radiative cooling below ambient air temperature under direct sunlight. Nature 2014;515:540–4

Appendix D

Latex Word Count

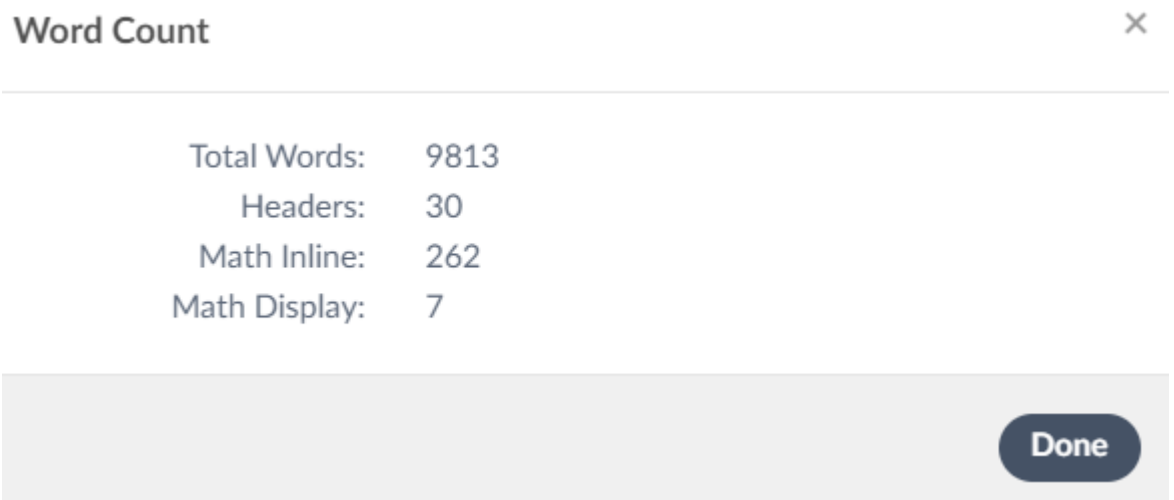

Figure D.1: Word count from Overleaf.